CHAPTER 1

Overview of Chemical Vapour Deposition

ANTHONY C. JONES[a] AND MICHAEL L. HITCHMAN[b]

[a] Department of Chemistry, University of Liverpool, Crown Street, Liverpool, L69 7ZD, UK; [b] Thin Film Innovations Ltd., Block 7, Kelvin Campus, West of Scotland Science Park, Glasgow, G20 0TH, UK

1.1 Basic Definitions

In the broadest sense chemical vapour deposition (CVD) involves the formation of a thin solid film on a substrate material by a *chemical reaction* of vapour-phase precursors. It can thus be distinguished from physical vapour deposition (PVD) processes, such as evaporation and reactive sputtering, which involve the adsorption of atomic or molecular species on the substrate. The chemical reactions of precursor species occur both in the gas phase and on the substrate. Reactions can be promoted or initiated by heat (thermal CVD), higher frequency radiation such as UV (photo-assisted CVD) or a plasma (plasma-enhanced CVD). There is a sometimes bewildering array of acronyms covered by the overall cachet of CVD and the interested reader is referred to several reviews.[1–4] Some of the more commonly used acronyms are defined below.

Metal-organic chemical vapour deposition (MOCVD) is a specific type of CVD that utilizes metal-organic precursors. In the strictest sense a metal-organic (or organometallic) compound contains a direct metal–carbon bond (σ or π) (*e.g.* metal alkyls, metal carbonyls). However, the definition of MOCVD has broadened to include precursors containing metal–oxygen bonds (*e.g.* metal-alkoxides, metal-β-diketonates) or metal–nitrogen bonds (*e.g.* metal alkylamides), and even metal hydrides (*e.g.* trimethylamine alane).

Metal-organic vapour phase epitaxy (MOVPE) or organometallic vapour phase epitaxy (OMVPE) is an MOCVD process that produces single crystal (*i.e.* epitaxial) films on single crystal substrates from metal-organic precursors. In MOCVD and MOVPE gas-phase reactions can sometimes play a significant role in the deposition chemistry.

Plasma-assisted or plasma-enhanced CVD (PECVD) is a technique in which electrical energy rather than thermal energy is used to initiate homogeneous reactions for the production of chemically active ions and radicals that can participate in heterogeneous reactions, which, in turn, lead to layer formation on the substrate. A major advantage of PECVD over thermal CVD processes is that

Chemical Vapour Deposition: Precursors, Processes and Applications
Edited by Anthony C. Jones and Michael L. Hitchman

Published by the Royal Society of Chemistry, www.rsc.org

deposition can occur at very low temperatures, even close to ambient, which allows temperature-sensitive substrates to be used.

Atomic layer deposition (ALD), sometimes called atomic layer epitaxy (ALE), alternatively-pulsed CVD, or atomic layer chemical vapour deposition (ALCVD), is a modification of the CVD process in which gaseous precursors are introduced sequentially to the substrate surface and the reactor is purged with an inert gas, or evacuated, between the precursor pulses. The chemical reactions leading to film deposition in ALD occur exclusively on the substrate at temperatures below the thermal decomposition temperature of the metal-containing precursor and gas-phase reactions are unimportant.

Chemical beam epitaxy (CBE) is high vacuum CVD technique that uses volatile metal-organic precursors and gaseous co-precursors. The closely related technique of metal-organic molecular beam epitaxy (MOMBE) uses volatile metal-organic precursors and co-precursor vapour derived from the solid element. In CBE and MOMBE the chemical reactions occur only on the substrate, leading to single crystal films and so gas-phase reactions play no significant role in film growth. Section 1.3 gives a more detailed description of these processes.

1.2 Historical Perspective

In common with many technologies, developments in CVD have largely arisen out of the requirements of society. These developments have been most rapid when other thin film deposition technologies have proved problematic or inadequate, for instance in the production of multiple thin films, as in modern semiconductor devices, or when the coating of large surface areas is required, as in large-scale functional coatings on glass. Several excellent reviews describe the historical development of CVD processes,[2,5,6] and the published literature from the earliest days to the mid-1960s is covered by a comprehensive review by Powell *et al.*[7] Therefore, this section gives only a brief description, highlighting some key advances.

Probably the earliest patent describing a CVD process was taken out by a certain John Howarth, for the production of "carbon black" for use as a pigment. Unfortunately, due to rather lax health and safety standards, the process only succeeded in burning down the wooden plant.[8] The early electric lamp industry provided another early impetus for CVD, and a patent issued in 1880 to Sawyer and Mann describes a process for the improvement of carbon fibre filaments.[9] However, these proved too fragile and later patents describe CVD processes for the deposition of various metals to produce more robust lamp filaments.[10,11]

One of the earliest examples of the CVD of metals is the deposition of tungsten, reported as early as 1855. Wöhler used WCl_6 with hydrogen carrier gas to deposit tungsten metal.[12] Later in the century (1890), the famous Mond Process was developed. This describes the deposition of pure nickel from nickel tetracarbonyl, $Ni(CO)_4$,[13,14] and was used for the refinement of nickel ore.[15]

The first reports of the deposition of silicon by CVD by the hydrogen reduction of $SiCl_4$ appear as early as 1909[16] and 1927,[17] and the widespread use of thin silicon films in the electronics industry is anticipated by the CVD of Si-based photo cells[18] and rectifiers[19] just after World War II.

During the late 1950s, triisobutylaluminium, $[Bu^t_3Al]$ began to be used extensively to catalyze the polymerization of olefins by the Ziegler–Natta process. At around the same time, it was found that the pyrolysis of $[Bu^t_3Al]$ gave high purity Al metal (>99 at.%). This led to its use in the early 1980s as a CVD precursor to Al metal for very large scale integration (VLSI) applications.[20,21] In patent literature of the late 1960s, aluminium trihydride (AlH_3, alane) was found to be useful for plating Al films from the vapour phase and by electroless deposition,[22–24] which led to the much later use of alane adducts such as $[AlH_3(NMe_3)]$ as CVD precursors for high purity Al thin films.[25] The reader is referred to Chapter 7 (Section 7.3) for recent developments in Al CVD.

Another important development in the history of CVD was the introduction of "on-line" CVD architectural coatings by Pilkington (now NSG Group). These coatings are deposited on a very large scale by atmospheric pressure CVD on a float glass production line.[26] By applying the coating directly to the float glass manufacturing line, economies of scale and production are achievable that are not possible with "off-line" deposition processes such as sputtering. Perhaps the most notable of these is fluorine-doped tin oxide, [SnO_2:F] developed by Pilkington in the mid-1980s ("Pilkington K-Glass"). This is a low thermal-emissivity (low–E) coating on windows, which prevents heat loss from the home and is essential to modern ecological energy saving efforts (Chapter 10, Section 10.1.1). It can be deposited using precursors such as [Me_4Sn], [$SnCl_4$] with halo-fluorocarbons or HF (Chapter 10, Section 10.2.2). A much more recent commercial product of Pilkington is "self-cleaning" glass. This has been coated on-line with a thin transparent film of TiO_2, and this chemically breaks down dirt by photocatalysis in sunlight (Chapter 10, Section 10.6).

Despite the various developments in CVD described above, the major impetus to the technology has undoubtedly been provided by the rapid development of the microelectronics industry since the mid-1970s. This has led to a requirement for very thin high purity films with precise control of uniformity, composition and doping.

Thin epitaxial films of n- or p-doped Si are the basic requirement for all Si integrated circuit technology. One of the earliest reports of silicon epitaxy was the closed tube transport of SiI_4 produced by heating solid Si in the presence of iodine.[27] Epitaxial Si films were later produced in the 1970s on a large commercial scale by the pyrolysis of monosilane (SiH_4) in H_2.[28]

Interest in the use of metal-organic compounds for CVD applications began in the early 1960s. The first reported preparation of a III-V material from a Group III metal-organic and a Group V hydride was by Didchenko *et al.* in 1960, who prepared InP in a closed tube by the thermal decomposition at 275–300 °C of a mixture of [Me_3In] and liquid [PH_3].[29] Next, in 1962, Harrison and Tomkins produced InSb in a closed tube by heating a mixture of [Me_3In] and [SbH_3] at 160 °C, and they also produced GaAs by heating a mixture of [Me_3Ga] and [AsH_3] at 200 °C.[30] In 1961 and 1965 patent applications by the Monsanto Co. claimed methods of depositing III-V compounds "suitable for use in semiconductor devices".[31,32] The processes involved the pyrolysis of volatile Group III and Group V compounds in an open tube system on a cubic crystal substrate to produce epitaxial films.

However, the Monsanto applications were of a rather general nature, listing a large range of volatile Group III compounds, and the few specific process examples given mainly involved Group III trihalides. In 1968, Manasevit and co-workers at the Rockwell Corporation gave the first clear description of the use of metal-organic compounds for the chemical vapour deposition of III-V materials. The first publication describes the deposition of GaAs by pyrolysis of a gas phase mixture of [Et_3Ga] and [AsH_3] in an open tube system using H_2 as the carrier gas.[33] Manasevit named the technique metal-organic chemical vapour deposition (MOCVD) and a patent was later filed for the MOCVD of a range of III-V materials and wide band-gap compound semiconductors.[34]

The emphasis in Manasevit's early work was on growth of non-epitaxial films on insulating substrates such as sapphire and spinel. However, in 1969 the growth of epitaxial GaAs on a GaAs substrate by metal-organic vapour phase epitaxy (MOVPE) was demonstrated.[35] Subsequently, a wide range of III-V compounds were deposited by MOCVD (or MOVPE), including AlGaAs,[36] InP, InAs, InGaAs,InAsP,[37,38] GaN and AlN,[39] although semiconductor device quality III-V materials still had not been produced. This was due largely to low purity precursors (often obtained from commercial suppliers of metal-organics for catalysis applications) and non-optimized MOCVD reactors and processes. In 1975, however, high-purity device quality GaAs films were grown[40] that had a low residual carrier concentration of $n = 7 \times 10^{13}\,cm^{-3}$ and high electron mobility ($\mu_{77K} = 120\,000\,cm^2\,V^{-1}\,s^{-1}$) (Section 1.7.2.4). Conventional techniques for the deposition of III-V materials such as liquid phase epitaxy (a combined melt of the components) proved incapable of producing the very thin multilayer structures required for efficient III-V devices and so MOVPE technology developed with ever increasing pace, and state-of-the-art GaAs photocathodes and field effect

transistors (FETs) were soon produced,[41] as well as complex multilayer structures such as AlGaAs/GaAs/AlGaAs double heterojunction lasers.[42] A particularly significant advance in III-V technology was the discovery of how to p-dope GaN-based semiconductors grown by MOVPE[43] (Chapter 6, Section 6.6.4.1) as this spawned the growth of a large industry in full-colour high-brightness light emitting diodes for energy efficient displays (Chapter 13, Section 13.7).

The reader is referred to Chapter 6 for a detailed description of the MOCVD of III-V compound semiconductor materials, including (Section 6.3.1) further details on the historical development of the technology. In many ways this is now a mature technology, more the province of salesmen and chemical buyers than development scientists, and commercial developments in this technology are described in Chapter 13.

The discovery of high-T_c superconducting oxides in the mid-1980s led to intense efforts to prepare these materials as thin films. This led to the development, beginning in the late 1980s,[44] of MOCVD techniques for the deposition of oxides such as $YBa_2Cu_3O_{7-\delta}$, and other superconducting oxides.[45] The difficulty in transporting low volatility metal precursors was largely responsible for the introduction of liquid injection MOCVD (Section 1.5 Figure 1.15). There has also been a great deal of effort devoted to the MOCVD of ferroelectric oxides such as $Pb(Zr,Ti)O_3$ and $SrBi_2Ta_2O_9$, and early reports date back to the early 1990s.[46] More recent advances in the MOCVD of a range of ferroelectric oxide materials are given elsewhere[47] and in Chapter 8 (Section 8.4).

The rapid recent advances in Si integrated circuit technology have largely been achieved by aggressive shrinking or "scaling" of devices such as metal oxide semiconductor field effect transistors (MOSFETS) and dynamic random access memories (DRAMs) (Chapter 8, Section 8.3, and Chapter 9, Section 9.2.2 and Figure 9.2). This has led to a requirement for new high-permittivity (or high-κ) oxide insulating materials to replace the conventional SiO_2 insulating or capacitor layers. PVD techniques can not give the desired deposition control of the very thin films required, or the necessary step coverage in high aspect-ratio device structures such as trench- and stack-structured DRAMs. Therefore, over the last few years there has been an intense effort to develop CVD processes for the deposition of high-permittivity metal oxides, such as Al_2O_3, ZrO_2, HfO_2, Zr- and Hf-silicate and the lanthanide oxides, and many CVD developments in this area are also detailed in Chapter 8 (Section 8.3).

Shrinking device dimensions also make it necessary to modify existing multilevel metallization technologies. This has led to recent efforts to deposit Al and Cu by MOCVD (Chapter 7, Sections 7.3 and 7.4), as well as stimulating research into the MOCVD of diffusion barriers such as TiN and TaN (Chapter 9, Sections 9.3.1 and 9.3.2).

Atomic layer deposition (ALD) was first introduced by T. Suntola and co-workers in the early 1970s,[48,49] and was initially used for the manufacture of luminescent and dielectric films required in electroluminescent displays (Chapter 4, Section 4.5.1).[50,51] More recently, ALD has been used to deposit the very thin conformal oxide films required as gate insulators in CMOS technology and in DRAM capacitor layers; see Chapters 4 (Section 4.5.3) and 8 (Section 8.3).

It is impossible to do justice here to the huge volume of research and development carried out on CVD over the past 100 years or so, but hopefully this brief survey gives a flavour of the great advances made.

1.3 Chemical Vapour Deposition Processes

1.3.1 Conventional CVD Processes

CVD processes are extremely complex and involve a series of gas-phase and surface reactions. They are often summarized, though, by overall reaction schemes, as illustrated in Scheme 1.1.

An overall reaction scheme tells us little about the physicochemical processes and the gas-phase and surface reactions involved. A more informative illustration of a CVD process is illustrated by

$$[Me_3Ga]_{(g)} + [AsH_3]_{(g)} \xrightarrow{500-700^{\circ}C} GaAs_{(s)} + 3CH_{4(g)}\uparrow$$

$$[SiH_4]_{(g)} \xrightarrow{500-800^{\circ}C} Si_{(s)} + 2H_{2(g)}\uparrow$$

$$[SiH_4]_{(g)} + O_{2(g)} \xrightarrow{350-475^{\circ}C} SiO_{2(s)} + 2H_{2(g)}\uparrow$$

$$2[Ta(OEt)_5]_{(v)} + 5H_2O_{(v)} \xrightarrow{350-450^{\circ}C} Ta_2O_{5(s)} + 10EtOH_{(v)}\uparrow$$

$$[NbCl_5]_{(v)} + 5/2H_{2(g)} + \tfrac{1}{2}xN_{2(g)} \xrightarrow{960^{\circ}C} NbN_{x(s)} + 5HCl_{(v)}\uparrow$$

Scheme 1.1 Overall reaction schemes for a variety of CVD processes.

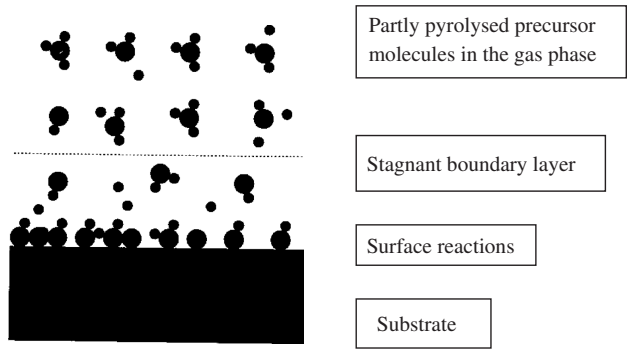

Figure 1.1 Simple schematic representation of the MOCVD process. (After ref. 52, Copyright John Wiley & Sons Limited, 1992. Reproduced with permission.)

the simple schematic[52] for an MOCVD reaction carried out at moderate pressures (*e.g.* 10–760 Torr) shown in Figure 1.1. A significant feature of the process is the presence of a hot layer of gas immediately above the substrate, termed the ''boundary layer'', and at these pressures gas-phase pyrolysis reactions occurring in the layer play a significant role in the MOCVD deposition process.

A more detailed picture of the basic physicochemical steps in an overall CVD reaction is illustrated in Figure 1.2, which indicates several key steps[4]:

1. Evaporation and transport of reagents (*i.e.* precursors) in the bulk gas flow region into the reactor;
2. Gas phase reactions of precursors in the reaction zone to produce reactive intermediates and gaseous by-products;
3. Mass transport of reactants to the substrate surface;
4. Adsorption of the reactants on the substrate surface;
5. Surface diffusion to growth sites, nucleation and surface chemical reactions leading to film formation;
6. Desorption and mass transport of remaining fragments of the decomposition away from the reaction zone.

In traditional thermal CVD, the film growth rate is determined by several parameters, the primary ones being the temperature of the substrate, the operating pressure of the reactor and the composition and chemistry of the gas-phase. The dependence of film growth rate on substrate temperature is typified by the growth of GaAs by MOCVD using $[Me_3Ga]$ and $[AsH_3]$[53,54] (Figure 1.3).

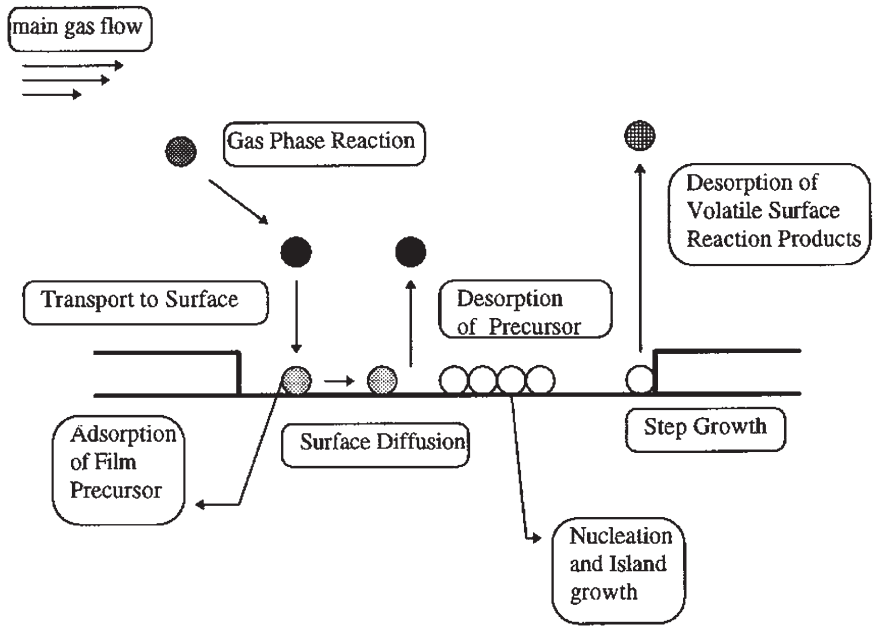

Figure 1.2 Precursor transport and reaction processes in CVD. (After ref. 4, p. 31, Copyright Wiley-VCH Verlag GmbH & Co. KGaA, 1997. Reproduced with permission.)

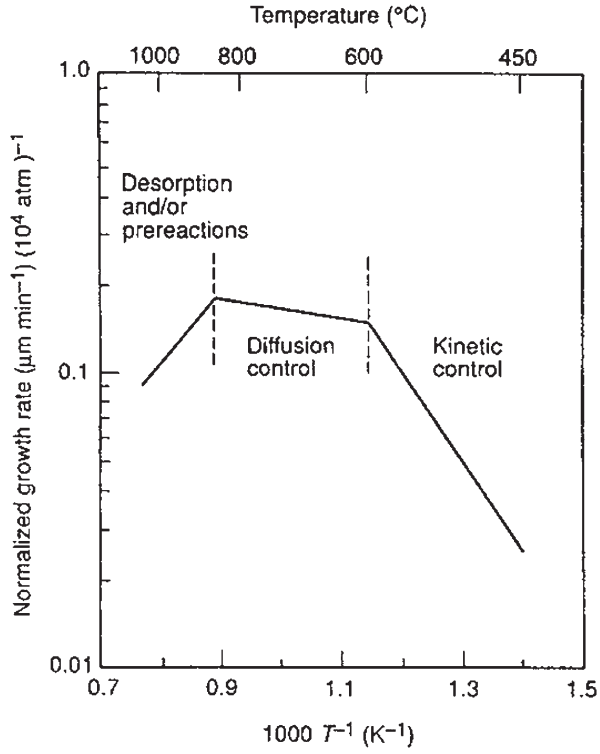

Figure 1.3 Plot of the normalized MOCVD growth rate of GaAs as a function of growth temperature. (After ref. 53, Copyright John Wiley & Sons Limited, 1987. Reproduced with permission.)

In this plot, of log of growth rate *vs.* reciprocal thermodynamic temperature, three regions are apparent. At lower growth temperatures the growth rate is controlled by the kinetics of chemical reactions occurring either in the gas-phase or on the substrate surface. This region is generally termed the region of *kinetic growth control* and the film growth rate increases exponentially with substrate temperature according to the Arrhenius equation:

$$\text{Growth rate} \propto \exp(E_A/RT) \tag{1.1}$$

where E_A is the apparent activation energy, R is the gas constant and T is the temperature. As the film growth rate is controlled by chemical kinetics, uniform film thickness can be achieved by minimizing temperature variations over the substrate surface, and this is the region utilized in hot-wall batch reactors used for the commercial production of Si epitaxial wafers by low pressure CVD.

As the temperature increases, the growth rate becomes nearly independent of temperature and is controlled by the mass transport of reagents through the boundary layer to the growth surface, and this is termed the region of *mass transport* or *diffusion-controlled* growth.

At even higher temperatures, the growth rate tends to decrease, due to an increased rate of desorption of film precursors or matrix elements from the growth surface and/or depletion of reagents on the reactor walls due to parasitic gas-phase side reactions. Gas-phase reactions become increasingly important with increasing temperature and higher partial pressures of the reactants.

Notably, Figure 1.3 is rather misleading in that it suggests there are sharp changeovers between the various regions. This is because of the nature of the plot where the log of the growth rate is used. If the growth rate itself were plotted then a much more gradual transition from one rate controlling step to the next would be seen.[2] An Arrhenius type plot as in Figure 1.3 has to be used with caution to obtain an activation energy for a kinetic process since there will be a contribution from mass transport. The slope of the ''kinetic region'' will not give a true value of the activation energy, but a lower value. Also, the ordinate contains the growth rate that is precursor concentration dependent and this may vary with temperature so, again, a true value of the activation energy will not be given from the slope of the ''kinetic region''.

A crucial factor that determines the relative importance of each regime is the pressure of the CVD reactor. From atmospheric pressure (760 Torr) to intermediate pressures (*e.g.* 10 Torr) gas phase reactions are important and, in addition, a significant boundary layer is present. Kinetics and mass transport can both play a significant role in deposition. As the pressure falls gas phase reactions tend to become less important, and particularly at pressures below 1 Torr layer growth is often controlled by surface reactions. At very low pressures (*e.g.* $< 10^{-4}$ Torr) mass transport is completely absent and layer growth is primarily controlled by the gas and substrate temperature and by desorption of precursor fragments and matrix elements from the growth surface.

A much more detailed discussion of the modelling of CVD processes is given in Chapter 3, and in Chapter 6 there is a detailed description of the chemistry (Section 6.3.2), thermodynamics, kinetics and hydrodynamics (Section 6.3.3) involved in III-V MOCVD technology.

1.3.2 Variants of CVD

As the brief historical overview of CVD given in Section 1.2 shows, CVD has gone through wide-ranging developments over the years. Since most CVD reactions are thermodynamically endothermic and they also have a kinetic energy of activation then energy has to be supplied to the reacting system. Traditionally, CVD processes have been initiated by a thermal energy input, which

can be inputted by several methods, *e.g.*:

- direct resistance heating of the substrate or substrate holder;
- rf induction of the substrate holder or susceptor;
- thermal radiation heating;
- photoradiation heating.

The use of thermal CVD can, however, be disadvantageous. For example, heat input can result in damage to temperature-sensitive substrates and so alternative forms of energy input have been developed which allow deposition at lower temperatures.

One way of reducing growth temperatures is to use plasma-assisted or plasma-enhanced CVD (PECVD).[55] With this technique deposition can occur at very low temperatures, even close to ambient, since electrical energy rather than thermal energy is used to initiate homogeneous reactions for the production of chemically active ions and radicals that can participate in heterogeneous reactions, which, in turn, lead to layer formation on the substrate. In non-thermal plasmas, which are typically generated by electrical discharges in the gas phase, the electron temperature is much higher than the gas temperature and inelastic collisions of the electrons with precursor molecules form the chemically active species. In addition, surfaces in the plasma can be bombarded with ions, electrons and photons, leading to changes in surface chemistry. Although PECVD usually allows lower temperature deposition than thermal CVD, the plasma bombardment of a surface often causes some substrate heating. PECVD processes have been widely used for the deposition of a large range of materials with standard and novel properties; both inorganic and organic materials, as well as polymers, have been prepared by the technique. There are complications, though, with PECVD, including plasma damage of the substrate and the growing film, and a strong process dependency on several parameters such as rf power and frequency, gas pressure, reagent flow rate, reactor geometry, *etc*. Chapter 12 reviews PECVD technology and its applications.

Another method of inputting energy to a CVD process is to use high energy photons. The process of photo-assisted CVD[56] involves interaction of light radiation with precursor molecules either in the gas phase or on the growth surface. Precursor molecules must absorb energy, and since traditionally simple inorganic precursors have been employed this necessitates the use of UV radiation. If more complex molecules are used as precursors, then photosensitizing agents may need to be added. The use of organometallic precursors (with π- and σ-bonded moieties) opens up the possibilities for a wider range of wavelengths, but this can lead to an increased potential for carbon incorporation. Photo-assisted CVD has similar potential advantages to those of PECVD; namely, low temperature deposition, modifications of properties of grown layers, *e.g.* dopant incorporation, and independent control of substrate temperature and dissociation of precursor. In addition, though, with masking or laser activation it is possible to achieve selected area growth. Chapter 11 considers photo-assisted CVD processes in detail.

A rather different variation of CVD is atomic layer deposition (ALD) and the specialist version atomic layer epitaxy (ALE).[57] In this modification of CVD, gaseous precursors are introduced alternately to the reaction chamber, where they reach a saturated adsorption level on the substrate surface. Introduction of the precursors is separated other by an inert gas purge, which removes any excess precursor molecules and volatile by-products from the reaction chamber, thus preventing unwanted gas phase reactions. In marked contrast to traditional thermal CVD, which involves pyrolysis of precursor molecules, ALD proceeds through surface exchange reactions, such as hydrolysis, between chemisorbed metal-containing precursor fragments and adsorbed nucleophilic reactant molecules. A typical growth cycle in the ALD of a lanthanide oxide from a precursor [LnL_3] (*e.g.* L = Cp, OR) occurs in the sequence H_2O pulse/[LnL_3] pulse/N_2 purge/H_2O pulse/N_2 purge (Figure 1.4).

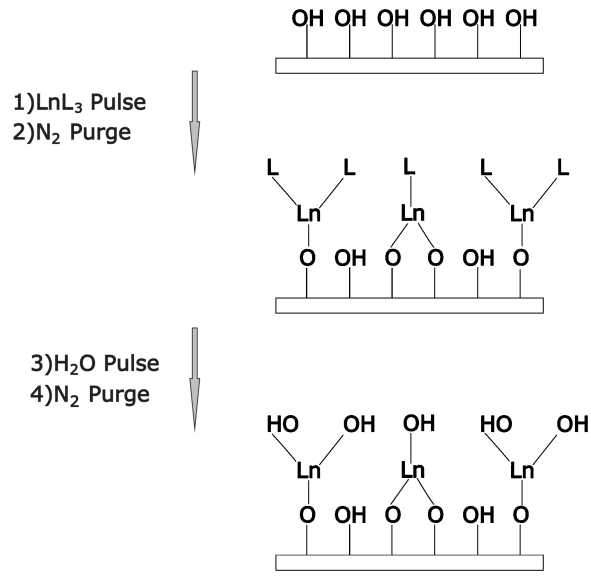

Figure 1.4 Schematic of an ALD growth cycle for deposition of a lanthanide oxide thin film from a lanthanide precursor [LnL_3] (*e.g.* L = Cp, OR) and H_2O.

In the first step a pulse of H_2O gives a reactive [OH]-terminated surface. A pulse of the LnL_3 precursor then leads to a chemisorbed [$(L)_2Ln–O–$] or [$(L)Ln–O_2–$] surface species, and the liberated LH species are removed by a N_2 purge. The surface is then effectively terminated with unreactive L groups and growth self-limits. The next H_2O pulse removes the remaining L groups and regenerates a reactive [OH]-terminated surface.

Under optimum conditions, film growth proceeds through self-limiting surface reactions of a saturated adsorbent in which one ALD cycle produces one monolayer of material. However, due to steric hindrance or lack of reactive surface sites, the growth rate per cycle is often considerably less than one monolayer. This is illustrated in Figure 1.4 where, for steric reasons, the large LnL_3 molecules are unable to react with all the surface-bound OH groups. Nevertheless, the growth rate per cycle is constant, so the thickness of the thin film can be controlled simply and accurately by varying the number of deposition cycles. Because ALD reactions occur exclusively on the substrate surface, the process can give superior step-coverage (or improved conformality) to traditional CVD, and so ALD has become the technique of choice for film deposition on very high-aspect ratio substrates. In ALD it is important that surface reactions predominate and that thermal decomposition of the precursor is minimized or avoided altogether, otherwise self-limiting growth will break down. ALD processes are, therefore, generally carried out at substrate temperatures in the region 200–350 °C, which is below the thermal decomposition temperature of most precursors. Chapter 4 (Section 4.2.1) gives a much more detailed discussion about ALD processes.

Chemical beam epitaxy (CBE) is a rather specialized CVD technique. This is a high vacuum process that uses volatile metal-organic precursors (*e.g.* a Group III metal alkyl) and gaseous co-precursors (*e.g.* AsH_3 or PH_3). The closely related technique of metal-organic molecular beam epitaxy (MOMBE) uses volatile metal-organic precursors and a co-precursor vapour derived from the solid element (*e.g.* As, P).[58,59] In CBE and MOMBE the chemical reactions occur only on the substrate surface and so gas-phase reactions play no significant role in the growth process. The use of CBE has perhaps declined somewhat in recent years, but its aims are to combine the advantages

of metal-organic vapour phase epitaxy (MOVPE) with those of molecular beam epitaxy (MBE). Since CBE is an ultrahigh vacuum (UHV) technique a potential advantage over conventional CVD is the ability to use vacuum *in situ* diagnostic techniques (*e.g.* RHEED, AES, MBMS) that provide real time analytical information on the growth process.

The growth kinetics of the CBE growth process are shown schematically in Figure 1.5, where it is compared to MOVPE and MBE processes.[60] Since CBE is an UHV technique, precursor desorption from the surface limits CBE growth processes to less than about 700 °C. It is therefore necessary to pre-pyrolyse thermally stable precursors. For example, in GaAs growth, thermally stable [AsH_3], has to be pre-decomposed to form the active surface species, As_2. A consequence of this is that there is a lack of active [AsH_x] species, which remove carbon-containing fragments in MOCVD,[61] and this leads to problems of carbon contamination in CBE.

There are still many other variants of CVD, but whatever the variant it is very apparent that, for a process to occur, starting materials, or precursors, are required, as is some form of reactor. The next two sections give a brief tour of these topics.

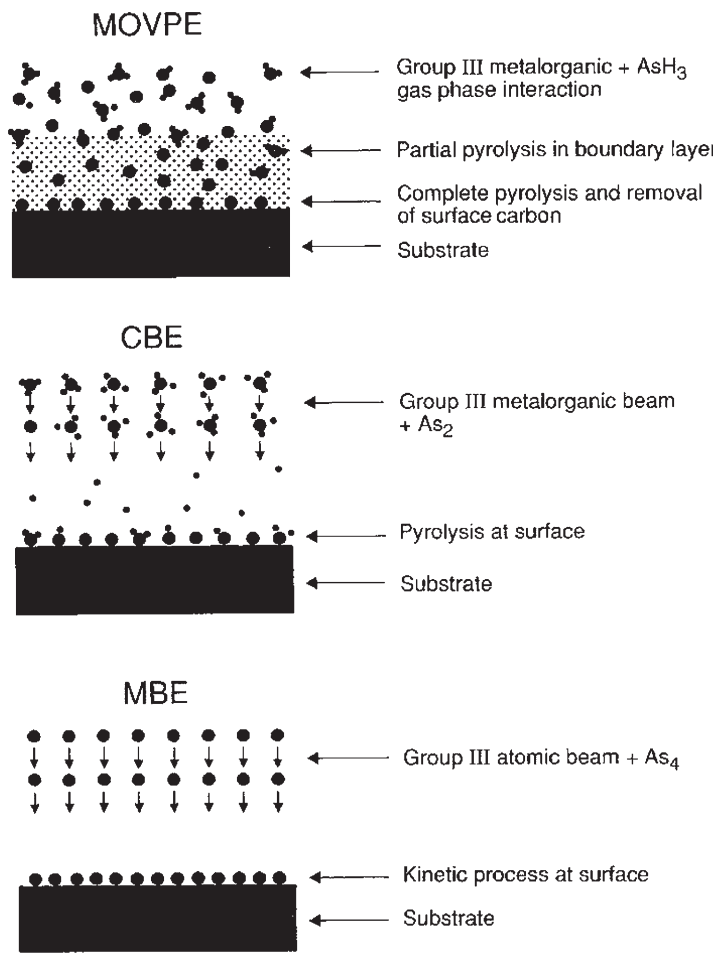

Figure 1.5 Schematic representation of the growth kinetics involved in MOVPE, CBE and MBE (molecular beam epitaxy, a PVD technique). (After ref. 60, Copyright John Wiley & Sons Limited, 1988. Reproduced with permission.)

1.4 CVD Precursors

1.4.1 Precursor Requirements

Whatever form a CVD process takes, the same precursor requirements generally apply. The characteristics of an "ideal" CVD precursor can be summarised as follows:

- Adequate volatility to achieve acceptable growth rates at moderate evaporation temperatures.
- Stability so that decomposition does not occur during evaporation.
- A sufficiently large temperature "window" between evaporation and decomposition for film deposition.
- High chemical purity.
- Clean decomposition without the incorporation of residual impurities.
- Good compatibility with co-precursors during the growth of complex materials.
- Long shelf-life with indefinite stability under ambient conditions, *i.e.* unaffected by air or moisture.
- Readily manufactured in high yield at low cost.
- Non-hazardous or with a low hazard risk.

Although these features are common for most CVD precursors, sometimes the precise precursor requirements can depend on the specific nature of the CVD process. For instance, in a traditional CVD processes it is a strong advantage if the precursor is relatively air-stable and not susceptible to reaction with water. This is a major disadvantage, though, in ALD, as it is essential that the surface exchange reaction with [OH] is facile, otherwise very low growth rates would result.

Another contrast between the requirements of a precursor for CVD in general and ALD is the size of the ligands attached to the central atom. In MOCVD, it is often advantageous to use very bulky ligands in the precursor, as this can often increase its vapour pressure, and also render it less air/moisture sensitive. In ALD, however, the presence of bulky or sterically demanding ligands around a precursor metal centre can lead to impractically low growth rates.

Also, a very high thermal stability (*e.g.* as in metal halides) can be a severe disadvantage in MOCVD, especially in microelectronics applications where low deposition temperatures ($< 500\,^{\circ}C$) are often required. In contrast, for ALD high thermal stability can be an advantage, as long as the precursor is reactive to H_2O or surface [OH] species, as this will lead to exchange reactions predominating over thermal decomposition reactions, as required for self-limiting growth. For examples of the very different requirements for MOCVD and ALD precursors see ref. 62.

The high vacuum environment of CBE leads to the added precursor requirement that it should ideally decompose cleanly by a unimolecular process, without incorporating excessive amounts of carbon in the film. This tends to lead to the use of Group II and Group III metal alkyls with alkyl ligands containing an easily-eliminated β-hydride atom (*e.g.* ethyl, *iso*-propyl, *etc.*).

Throughout this volume the characteristics of precursors will be referred to in a wide range of contexts, and most of the requirements outlined above will become apparent. Here, though, some particular aspects of precursor chemistry mentioned above are considered in more detail.

1.4.2 Precursor Volatility

The main requirement of any precursor is that it has an adequate volatility. With precursors that occur naturally in a gaseous state (*e.g.* silane, diborane, ammonia, *etc.*) this is not a problem. However, for precursors that are liquids or solids, volatility often has to be enhanced by a reduction of the intermolecular forces that lead to dimer, oligomer or polymer formation. Good

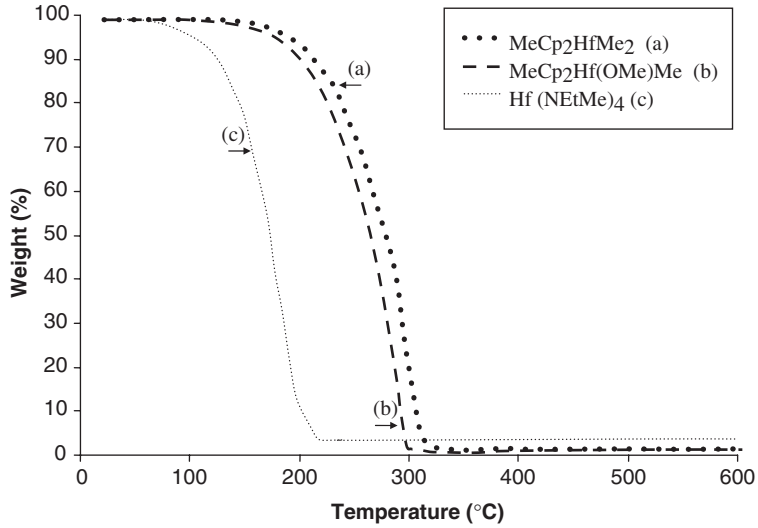

Figure 1.6 Thermogravimetric analytical (TGA) data for $[Hf(NEtMe)_4]$, $[(MeCp)_2HfMe_2]$ and $[(MeCp)_2Hf(OMe)Me]$.

examples of how this is achieved are given in Chapter 8 (Section 8.2) and Chapter 5 (Section 5.6.1) for metal oxide precursor chemistry where neutral complexes $[ML_n]$ are designed to have mono-anionic ligands that completely fill the coordination sphere of the metal.

The introduction of new chemicals into production processes can be an expensive, time consuming exercise. Therefore, a key parameter to ensure optimum process design is reliable precursor volatility data. A good idea of the temperature required to evaporate the precursor can be obtained by thermogravimetric analysis (TGA), in which the weight loss of a precursor is measured as a function of increasing temperature. Since many precursors are air sensitive they must be transferred to the TGA apparatus in an inert atmosphere, and hence the apparatus is generally enclosed in a nitrogen box. An example of the usefulness of TGA is illustrated by Figure 1.6, which shows the TGA data for three different precursors used in ALD, $[Hf(NEtMe)_4]$, $[(MeCp)_2HfMe_2]$ and $[(MeCp)_2Hf(OMe)Me]$ (Chapter 8, Section 8.3.1.2).

The TGA data show that the $[Hf(NEtMe)_4]$ complex evaporates in the temperature range $\sim$100–225 °C, leaving a small amount of residue ($\sim$2.5%), possibly due to trace air ingress during sample handling. The organometallic complexes $[(MeCp)_2Hf(OMe)Me]$ and $[(MeCp)_2HfMe_2]$ are clearly less volatile, evaporating in the ranges $\sim$150–300 °C and 150–320 °C, respectively. TGA data also provide information on precursor stability, with the presence of large amounts of residue indicating decomposition during evaporation.

However, although TGA is a useful indicator of precursor volatility and stability, it is no substitute for accurate vapour pressure determination. It is not a trivial excersise, though, to obtain accurate vapour pressure data, as shown by the large variation in literature values for even well-known precursors.[63–65] During vapour pressure measurements it is essential that the precursor is fully vapourized and that condensation of the precursor within the measurement equipment upstream of the pressure measurement device is avoided; this can be difficult, especially for low-volatility compounds. It is important too that the precursor is free from gaseous contaminants, deriving from precursor decomposition or from the inert gas blanket in the precursor storage container. It is also essential to calibrate the data for the precursor against a standard with a known accurately determined vapour pressure (*e.g.* naphthalene[66]). Figure 1.7 shows a schematic diagram

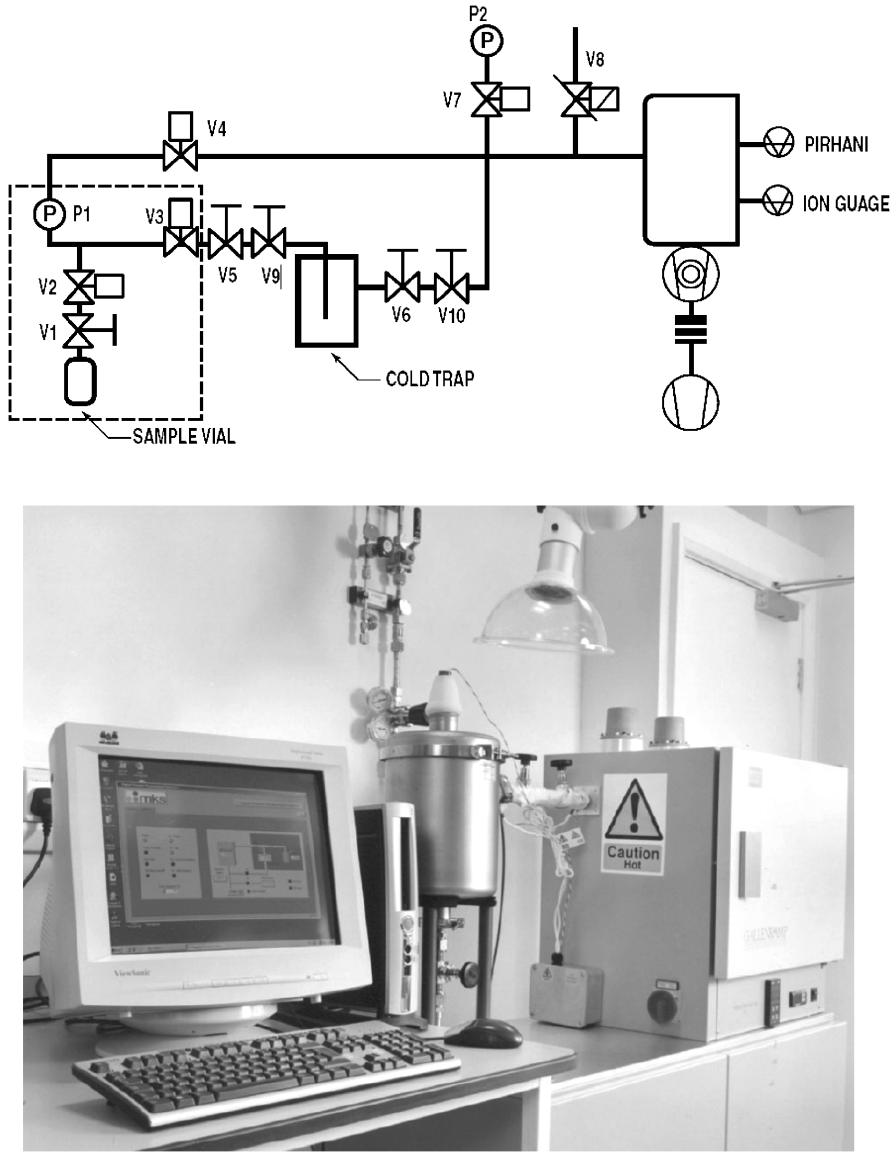

Figure 1.7 Apparatus used by a commercial manufacturer to accurately measure the vapour pressure of metalloorganic MOCVD and ALD precursors. (Reprinted from ref. 66, with permission from Elsevier.)

and photograph of a vapour pressure measurement system used by a commercial precursor manufacturer.[66] The instrument is constructed entirely of stainless steel with high integrity joints throughout. The key sections of the instrument are located inside an oven to prevent precursor condensation and vapour pressure is measured using a Baratron™ pressure gauge attached to a vacuum manifold.

The vapour pressure of the compound is measured at various temperatures (see Figure 1.8 for data for $[Ta(NMe_2)_5]$) and from a plot of $\log_{10}P$ against $1/T$ (in K) vapour pressures over a wide range of temperatures can be determined. The vapour pressure of $[Ta(NMe_2)_5]$ is given by Equation

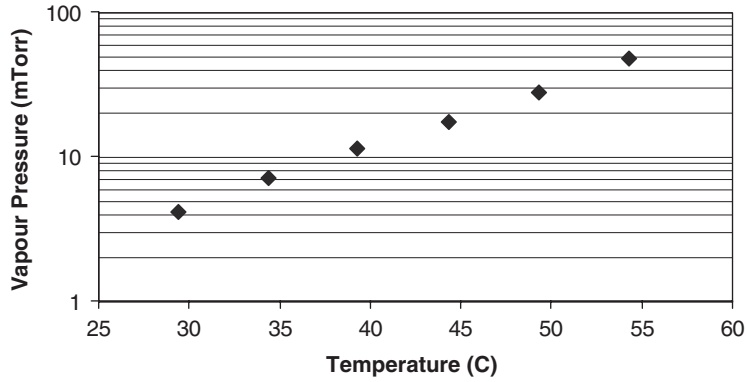

Figure 1.8 Vapour pressure data for $[Ta(NMe_2)_5]$. (Reprinted from ref. 66 with permission from Elsevier.)

(1.2),[66] which allows the calculation of vapour pressure at any specified temperature:

$$\mathrm{Log}_{10}P = -4124.9/T + 11.265 \tag{1.2}$$

Vapour pressure data for several metal oxide precursors are given in Chapter 8 (Table 8.5), while data for a selection of III-V semiconductor precursors are shown in Chapter 6 (Table 6.4).

1.4.3 Precursor Thermal Stability

As has been indicated earlier, thermal stability is also a crucial factor in determining the suitability of a precursor for CVD applications, and it is now routine for a commercial precursor manufacturer to carry out extensive thermal stability tests on their products. First, the precursor should be sufficiently stable for long-term storage at room temperature, and then it should not undergo any appreciable decomposition at the evaporation temperatures necessary to achieve adequate gas-phase transport. For safety reasons it is also essential to ensure that rapid thermal decomposition of a precursor does not occur by misuse or by accident, particularly when the precursor is manufactured and used in large multi-kilogram or ton quantities. In the case of some precursors, such as alane adducts (*e.g.* $[AlH_3(NMe)_3]$) – see Chapter 7 (Section 7.3.1.3) – poor storage practices can lead to decomposition, generating large volumes of gaseous products and pressures of hundreds of atmospheres in a sealed container.

Differential scanning calorimetry (DSC) is a common method of determining the thermal stability of precursors. DSC measures the difference in heat flux between a sample and a reference material as a function of temperature. Both the sample and reference material are subjected to a controlled temperature programme, and endothermal and exothermal changes in enthalpy can be observed. The heat changes reflect physical and/or chemical processes, such as phase transitions or chemical recations. Figure 1.9 shows a typical DSC curve for a CVD precursor, illustrating four common features commonly observed in DSC experiments.[67]

It can be seen that DSC provides information about the temperatures at which melting and decomposition begin (T_{onset},) and when the thermal event ends (T_{end}). T_{max} and T_{min} are the temperatures at the maximum of the exotherm and the minimum of the endotherm, respectively. The area under the exothermic and endothermic peaks are related to the total heat of reaction. These DSC parameters depend strongly on the rate of sample heating, with sample size being less critical, so that a low rate of heating ($\sim 2\,^{\circ}\mathrm{C\,min^{-1}}$) is generally used. Although it is difficult to

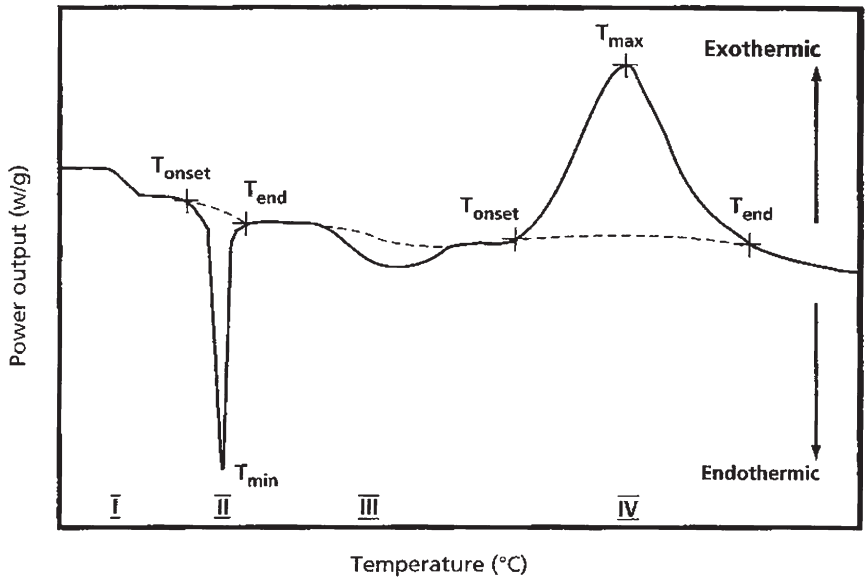

Figure 1.9 Typical DSC trace, illustrating four different types of transition: (I) a baseline shift caused by a glass transition; (II) an endothermal effect caused by melting; (III) an endothermal effect caused by dissociation of the compound; (IV) an exothermal effect caused by decomposition of the compound. (After ref. 67, Copyright John Wiley & Sons Limited, 1997. Reproduced with permission.)

derive absolute thermochemical values from DSC data, general trends in the thermal stability of CVD precursors can be established.[67]

1.4.4 Precursor Purity and Precursor Analysis

In any chemical process the purity of the reactants is of paramount importance. For thin film deposition by CVD this is especially true. The influence of precursor purity on the properties of the deposited film can be illustrated by considering the doping of III-V compound semiconductors (*e.g.* GaAs, InP), for which much work has been done on correlating impurity levels in the precursor with those in MOCVD-grown films, as described in an early review.[68] The presence of volatile trace metal impurities in the Group III metal-organic precursor (*e.g.* $[Me_3Ga]$, $[Me_3In]$) leads to the incorporation of shallow ionized impurities in the semiconductor layer. The energies of these impurities place them in the band gap of the III-V layer, and when introduced intentionally they lead to various sophisticated III-V devices, such as GaAs/AlGaAs/GaAs double heterojunction lasers and p/n doped GaN-based LEDs.

However, with unintentional doping the impurities can seriously degrade the properties of a III-V semiconductor by lowering the electron mobility through scattering,[69] and decreasing the photoluminescence by providing non-radiative recombination pathways.[70] GaAs and InP have intrinsic free charge carriers of $< 10^{13}\,cm^{-3}$, and it has been found that as little as 1 ppm of an unintentional dopant impurity in the layer corresponds to an impurity concentration of $2.5 \times 10^{16}\,cm^{-3}$, which is unacceptable for most device applications.

Unintentional dopants are generally introduced during precursor synthesis, as is the case of volatile metal-organic impurities in $[R_3Ga]$ or $[R_3In]$ precursors.[71] For instance, $[Me_3Ga]$ can be synthesized from the reaction between a Grignard reagent, such as [MeMgI], and $[GaCl_3]$ (Chapter 6, Section 6.5.1). Magnesium is thus a common impurity in the $[Me_3Ga]$, along with Si and Zn,

Table 1.1 Common dopants in III-V semiconductors.

Impurity elements	*Group*	*Site occupied*	*Electrical behaviour*	*Typical dopant precursors*
Be, Mg	II A	III A (Al, Ga, In)	p-type Shallow ionized acceptor	[Et_2Be], [Cp_2Mg], [$(MeCp)_2Mg$]
Zn, Cd	II B	III A (Al, Ga, In)	p-type Shallow ionized acceptor	[Me_2Zn], [Et_2Zn] [Me_2Cd]
C	IV A	V A (As, P)	p-type Shallow ionized acceptor	[CCl_4], [CBr_4] ($CH_3^{\bullet}$)radicals from [Me_3M] precursor
Si, Sn, Ge	IV A	III A (Al, Ga, In)	n-type Shallow ionized donor	[SiR_4], [SiH_4], [R_4Sn], [R_4Ge]
S, Se, Te	VI A	V A (As, P)	n-type Shallow ionized donor	[H_2S], [H_2Se], [R_2S], [R_2Se], [R_2Te]

which originate in the Mg and/or the $GaCl_3$. Table 1.1 shows some common dopants in III-V materials.

As shown in Table 1.1, these impurities generally act substitutionally, occupying a lattice site normally belonging to a Group III or V element, which has the net effect of adding an electron (n-type charge carrier) or hole (p-type charge carrier). The concentration of these impurities in the III-V film is often a strong function of growth temperature, for instance the level of the n-type dopants Si and Sn tends to increase with increasing growth temperature, whilst the level of others, such a the p-type dopants Zn, Mg and Cd, tends to decrease.

To minimize unintentional doping, highly sophisticated analytical techniques have been developed for the determination of trace metal impurities in metal-organic precursors, which are often highly reactive or even pyrophoric (*e.g.* [Me_3Ga], [Me_3In], and [Me_3Al]). The techniques include flameless atomic absorption spectrophotometry,[72] direct injection inductively coupled plasma optical emission spectroscopy (ICPOES) and ICP-mass spectrometry (ICPMS).[73] These techniques can detect impurities at the ppb level (see examples for [Me_3Al], Chapter 6, Tables 6.5 and 6.6). Table 1.2 shows a correlation between impurities in the metal-organic precursor and the electrical properties of a III-V layer.[68]

As well as trace metal impurities affecting layer characteristics, carbon and oxygen contaminants also play a crucial role in determining layer properties. Carbon impurities are inherent to MOCVD and CBE growth processes, originating from the thermal decomposition of the organic groups in the precursor, and the level of carbon incorporation is strongly dependent on the molecular structure of the precursor. Oxygen may be introduced at various stages of an MOCVD process, through, for example, volatile oxygen-containing impurities in the precursor (*e.g.* [Me_2AlOMe] in [Me_3Al]), or from leaks in the source container or reactor inlet lines. The presence of oxygen is a particular problem in optical devices containing Al in the active layer, as this can seriously degrade their optical efficiency. Organic impurities are, perhaps, more difficult to detect and quantify than metallic impurities in precursors. Mass spectrometry is useful for identifying hydrocarbon impurities,[68] whilst Fourier- transform (FT) NMR has been used to detect oxygen-containing organic impurities at the low ppm level (Chapter 6, Section 6.5.2 and Table 6.7). Finally, hydrogen, present in the metal-organic precursor and in the MOCVD process gases, can also influence semiconductor layer properties, by passivating intentional dopants such as Mg in GaN.

Table 1.2 Effect of precursor purity on the electrical properties of a GaAs layer.[68]

Group III precursor	*ICP-ES analysis*[a] *(ppm)*	*III-V material [growth temp. (°C)]*	*Electron carrier concentration*[b] *[η_{77K} (cm^{-3})]*	*Electron mobility*[b] *[μ_{77K} ($cm^2 V^{-1} s^{-1}$)]*
[Me_3Ga] Batch 1	Si 1.2, Zn 2.0	GaAs (650)	1.1×10^{15}	42 600
[Me_3Ga] Batch 2	Si < 0.03 Zn < 0.2	GaAs (650)	1.4×10^{14}	137 000

[a]No other impurities detected.
[b]Low η values and high μ values indicate that the layer is of high purity with few extrinsic impurities.

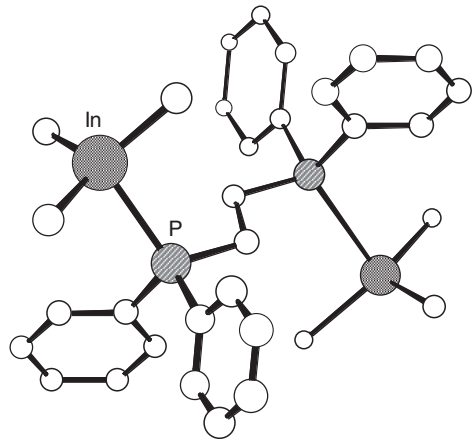

Figure 1.10 Crystal structure of the [$(Me_3In)_2 \cdot$ DIPHOS] adduct used to purify [Me_3In]. (Courtesy of the Cambridge Structural Database, see "The Cambridge Structural Database; a quarter of a million crystal structures and rising", F.H. Allen, *Acta Crystallogr., Sect. B: Struct. Sci.*, 2002, **58**, 380.)

1.4.5 Precursor Purification Techniques

The critical effect of precursor purity on layer properties, particularly in III-V MOCVD technology, has led to an intense effort to purify precursors to levels of up to 99.9999% purity (on a metal basis); the improvement of precursor purity, especially in the 1980s, played a critical role in the development of the compound semiconductor industry. Classical purification techniques[74] include sublimation, recrystallization, fractional distillation (or rectification),[75] preparative chromatography[76] and, for III-V precursors, distillation of the metal-organic compound from a reactive melt such as gallium[77] or sodium/potassium alloy.[78] The removal of trace metal and organic impurities from an organometallic compound can often be difficult using techniques such as distillation, especially when the contaminant has a similar boiling point to the organometallic compound (*e.g.* [R_4Si], [R_2Zn] *etc.*). This led to the development some years ago of "adduct-purification" techniques, which involve the formation of an involatile (Lewis acid–Lewis base) adduct as an intermediate in the purification process.[79,80] An example of this is the purification of trimethylindium by the formation of the [$(Me_3In)_2 \cdot$ DIPHOS] adduct (DIPHOS = 1,2-bis(diphenylphosphino)ethane) (Figure 1.10).[81] Volatile impurities such as diethyl ether solvent and trace metal contaminants such as [R_4Si] and [R_4Sn] which do not form adducts with DIPHOS can easily be removed under vacuum. Pure [Me_3In] is then obtained by thermal dissociation of the relatively weak [Me_3In]—[DIPHOS] bond and isolation by vacuum distillation[80] (Chapter 6, Section 6.5.1 and Figure 6.10).

The adduct purification process was also applied very successfully to [Me_3Ga] using adducts with high boiling ethers.[71,79]

1.5 CVD Reactors

A very large range of reactors and several different precursor delivery systems have been used in the various areas of CVD technology. These are dealt with in detail in Chapter 2, but it may be useful to begin with a brief and general overview of CVD reactors. Irrespective of the variations in CVD processes, all thermal CVD reactors have common features:

- Precursor sources.
- Gas handling system to control input of precursor gases or vapours to the reaction zone.
- A reaction zone, usually within an enclosed cell, with a holder that can accommodate the substrate, and which is heated by a surrounding oven or furnace, or by external radiofrequency or infrared radiation.
- An exhaust system, which may include a vacuum pump for low pressure operation, to remove waste products and a waste treatment facility with any necessary waste monitoring devices.

A schematic of a typical MOCVD reactor used to deposit a III-V material from a Group III trialkyl compound and a Group V hydride is shown in Figure 1.11 (taken from Chapter 6, Figure 6.8).

The volatile precursors are contained in separate containers, commonly called ''bubblers'', usually made of stainless steel (although quartz or Pyrex glass can also used). The bubbler is equipped with inlet and outlet bellows-sealed or diaphragm-sealed valves and a dip-tube attached to the inlet valve (Figures 1.12 and Ch. 6, Figure 6.9). Precursor transport is controlled by passing an inert carrier gas (*e.g.* H_2, Ar, N_2) through the precursor in the bubbler. A mass flow controller upstream of the bubbler can accurately control the rate of precursor transport. Ideally, the carrier gas should become fully saturated with precursor vapour, but this is not absolutely essential as long as the pick-up by the carrier gas is reproducible. To facilitate this, the bubblers are held in temperature-controlled baths. For the most careful deposition control, reactors are generally operated in ''vent-run'' mode, in which a vent line allows the flow of reactants to be stabilized before entering the reactor. When the reactant is required the manifold very rapidly switches the reactant flow into the reactor, and this can allow the growth of complex multilayer materials.

The flow into a reactor can be in a vertical or horizontal manner and schematic illustrations of some common reactor types are shown in Figure 1.13.[53] As mentioned earlier, various modes of heating can be employed.

Precursors used for some growth processes, such as III-V and II-VI semiconductors generally have high vapour pressures (>1 Torr), at moderate source temperatures, typically $<50\,^{\circ}C$.[82,83] However, for other processes, such as metal oxide MOCVD, many precursors have only very low vapour pressures of $\ll 1$ Torr close to room temperature, so that high evaporation temperatures are needed for efficient deposition. Several strategies have been employed to deal with this situation. The chemistry-based approach, mentioned earlier, is to design precursor molecules with reduced intermolecular forces to overcome oligomerization. An equipment-based approach is to have not just the precursor container heated but also the pipe-work to the reactor heated to a temperature high enough to prevent precursor condensation; this would typically be 20–30 °C above the bubbler temperature. Pipe-work can be heated by using co-axial tubing with a heat transfer reagent (*e.g.* oil) passing through the annular region (Figure 1.14),[84] or simply by wrapping heating tapes around the pipes.

Both approaches have been successfully used for the growth of several complex ferroelectric oxides such as $PbTiO_3$, $Pb(Zr,Ti)O_3$ and high-Tc superconducting oxides.[84,85] A problem remains, though, in that some metal oxide precursors, such as metal alkoxides or β-diketonates, have

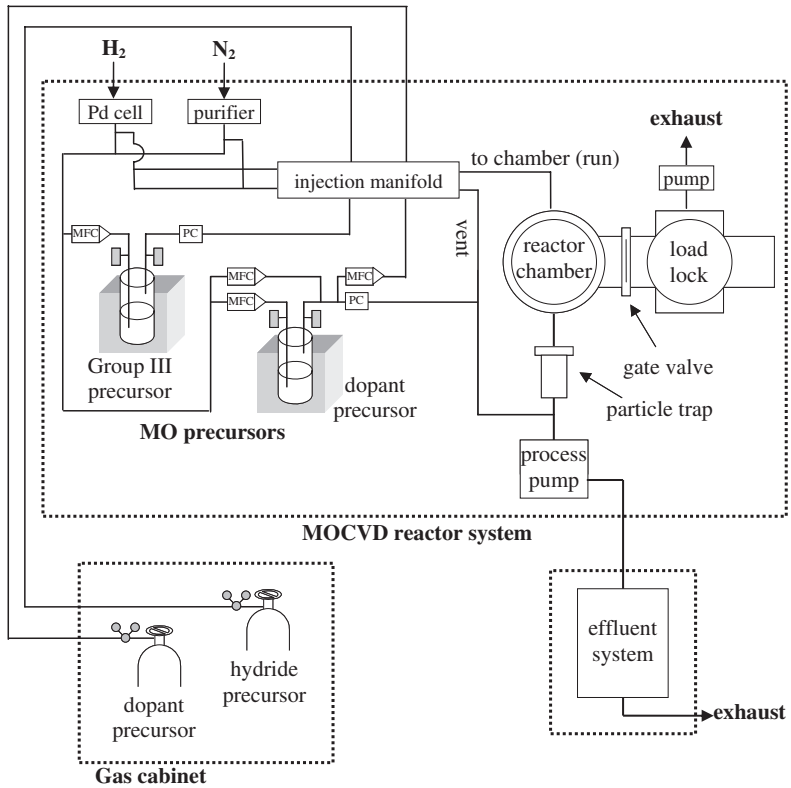

Figure 1.11 Schematic of a typical MOCVD reactor used for the deposition of III-V semiconductor films. Taken from Chapter 6 (Figure 6.8).

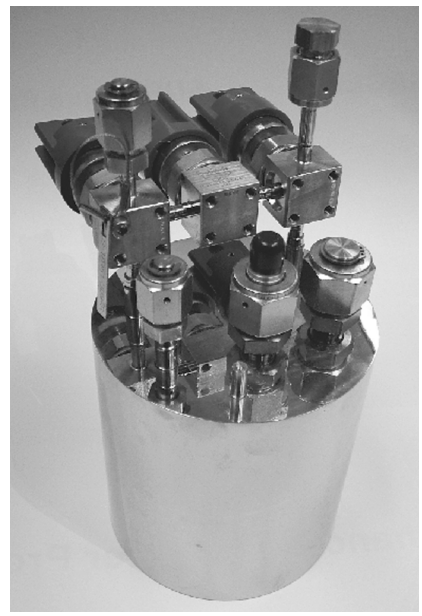

Figure 1.12 A commercial "bubbler" used to evaporate metal-organic compounds for MOCVD. (Courtesy of SAFC Hitech.)

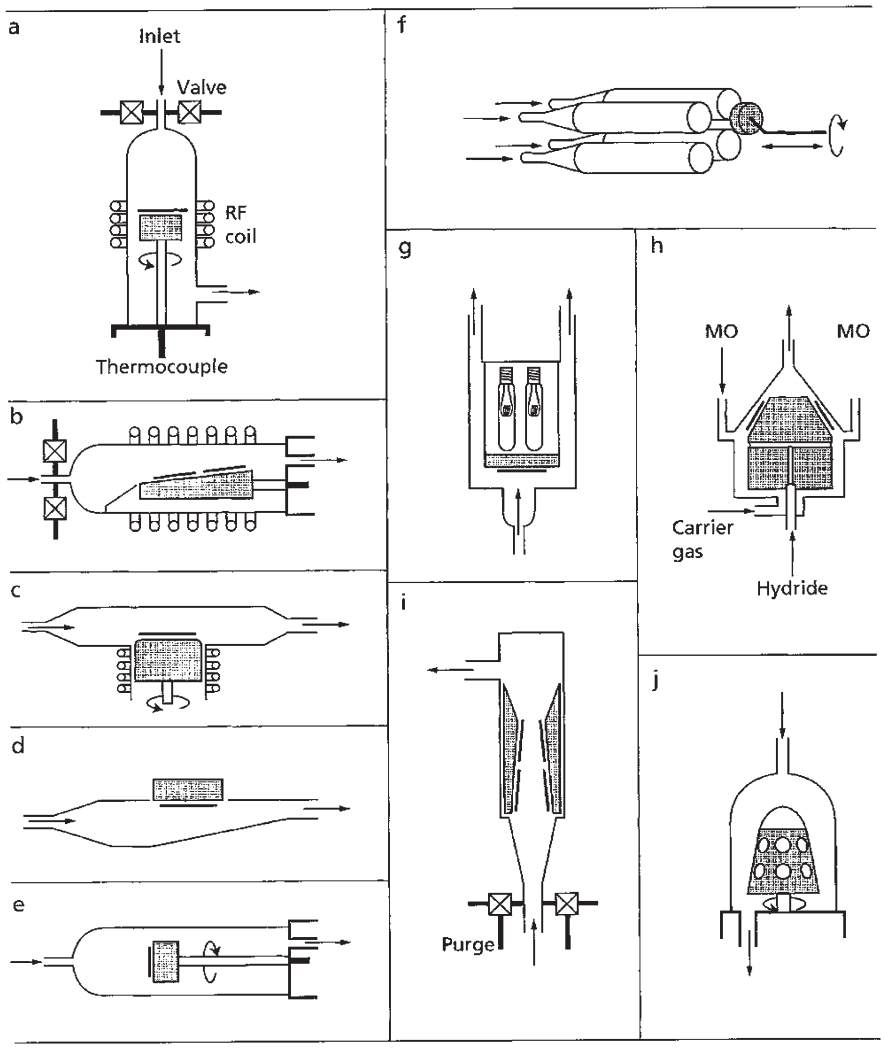

Figure 1.13 Some common reactor cell geometries used in MOCVD: (*a*) rotating disc, gas inlet at top, (*b*) horizontal reactor, (*c*) "T" reactor with rotating susceptor, (*d*) reactor with inverted wafer mounting, (*e*) horizontal reactor with substrate normal to gas flow, (*f*) multiple barrel reactor, (*g*) barrel-type reactor with separate inlets, (*h*) inverted stagnation point flow reactor, (*i*) chimney reactor, (*j*) large-scale barrel reactor. (After ref. 53, Copyright John Wiley & Sons Limited, 1987. Reproduced with permission.)

insufficient thermal stability to withstand heating for long periods. They can slowly decompose in the bubbler or in the inlet pipe-work, leading to poor oxide layer uniformity and reactor blockages, or undergo annealing and crystallization, so that carrier gas pick-up rates change with time. These problems associated with low volatility precursors can be largely overcome by the use of liquid injection MOCVD, in which the precursor is dissolved in an inert solvent, usually an ether (*e.g.* tetrahydrofuran) or a hydrocarbon (*e.g.* heptane or nonane).[47] The precursor solution is kept at room temperature and when required it is delivered at a precisely controlled rate and quantity into a heated evaporator and transported by a carrier gas into the reactor zone. For multi-component layers, separate precursor solutions can be used for growth, or several precursors can be dissolved

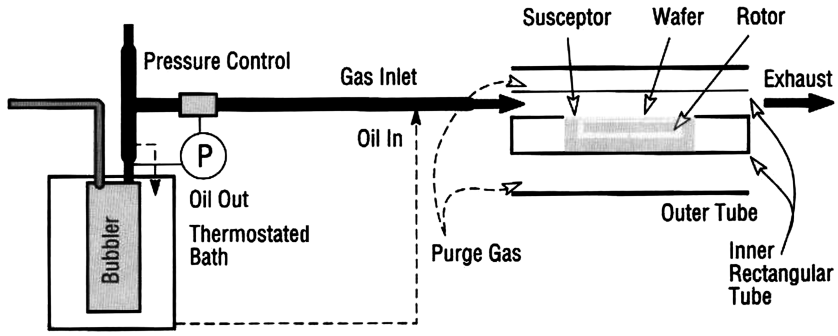

Figure 1.14 Schematic of a conventional MOCVD reactor with a heated delivery line used to deposit ferroelectric oxides [*e.g.* $Pb(Zr,Ti)O_3$] using low vapour pressure precursors. (After ref. 84. Reproduced by permission of the MRS Bulletin.)

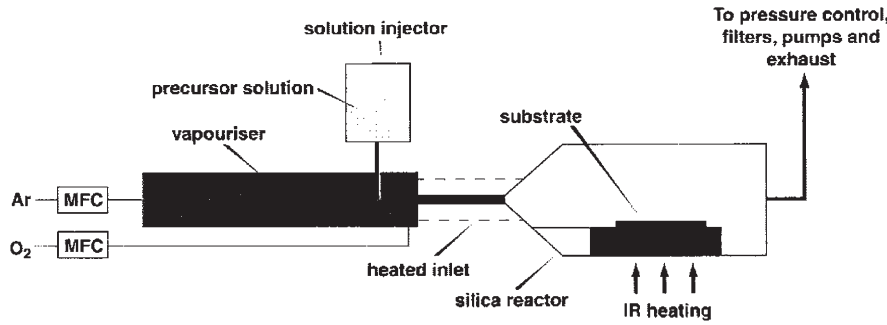

Figure 1.15 Schematic diagram of a simple liquid injection MOCVD reactor. (After ref. 47, reproduced by permission of The Royal Society of Chemistry.)

in an appropriate molar ratio in a single solution to form a "precursor cocktail". Figure 1.15 shows a schematic of a liquid injection MOCVD system.[47]

A potential disadvantage of liquid injection MOCVD is that the precursor solution is evaporated from a single heated evaporator, unlike in conventional MOCVD where each bubbler is separately heated. In liquid injection MOCVD it is therefore often necessary to select, or design, co-precursors that evaporate at similar temperatures.

In ALD a similar precursor delivery system to conventional CVD is generally used, but valves are added to shut off the precursor pulse or oxygen reactant pulse, and an inert gas purge line is added to remove materials desorbed during each ALD cycle. A full explanation of an inert gas valving system is given in Chapter 4 (Section 4.4).

With CBE, although film growth occurs in a UHV environment, the condensed phase metal-organic Group III precursors and gaseous Group V precursor are again held in containers external to the system. In this case, though, reagent flow into the growth chamber is in the molecular regime, allowing retention of the use of shutters, and *in situ* masks. An advantage of CBE is the use of *in situ* analytical equipment such as RHEED, mentioned above, and also of residual gas analysis for the detection of impurities. A typical CBE reactor is shown in Figure 1.16.[58,59]

Chapter 2 gives a highly detailed description of the large range of CVD reactors, injection systems and ancillary equipment, together with a discussion of gas dynamics, delivery systems and reactor cells.

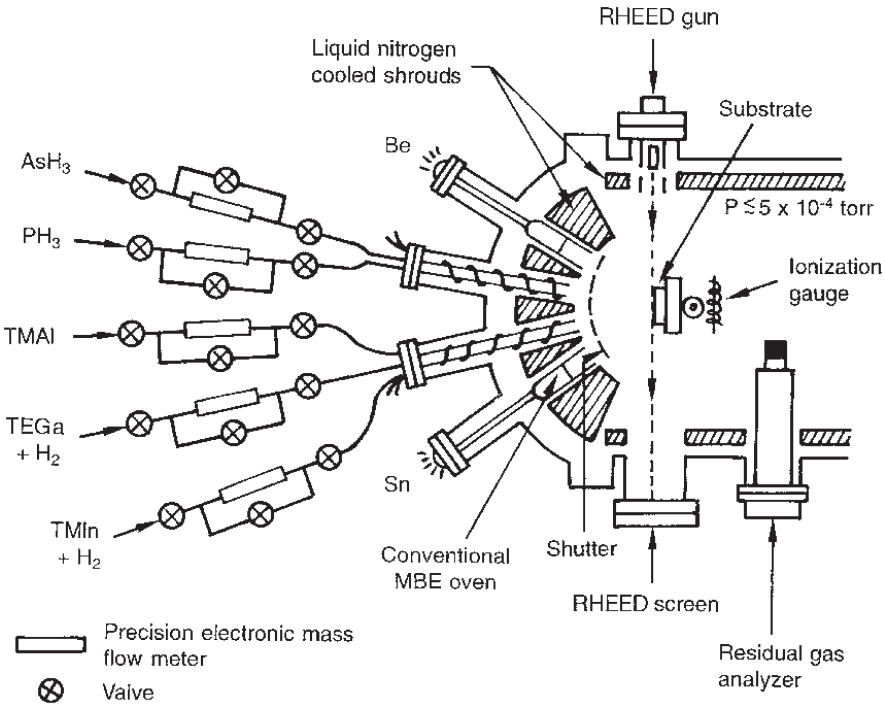

Figure 1.16 Schematic diagram of a typical CBE reactor system. (After ref. 60, Copyright John Wiley & Sons Limited, 1988. Reproduced with permission.)

1.6 Materials Deposited by CVD and Applications

A very extensive range of materials has been deposited using conventional CVD and its variants. These materials find applications in the following main areas of technology:

- microelectronics
- optoelectronics
- protective and decorative coatings
- optical coatings

Table 1.3 give examples of the classes of CVD-grown films, classified according to their chemical nature, together with applications and typical precursors used. The table is by no means exhaustive, but gives a good idea of the wide variety of precursors used in the various application areas of CVD. Although some precursors are more suited to a particular CVD technology (*e.g.* ALD rather than MOCVD), many of these precursors are utilized in all areas of the technology.

Detailed discussions of CVD grown materials are given in Chapters 4 and 5–12.

1.7 Materials Properties

1.7.1 Layer Morphology

Layer morphology is important in determining the physical characteristics and usefulness of a film. It is determined by surface diffusion and nucleation processes during deposition, which in turn are

Table 1.3 Selection of films grown by CVD, their applications and typical precursors used.

General class of material	*Specific material*	*Applications*	*Typical CVD precursors*
Dielectric oxides	TiO_2, ZrO_2, $ZrSi_xO_y$, HfO_2, $HfSi_xO_y$	High-κ gate dielectric layers in CMOS technology	Metal-β-diketonates (*e.g.* $[M(\beta\text{-dik})_4]$ (M = Zr, Hf), $[Ln(OR)_3]$, $[Ln(\beta\text{-dik})_3]$ (Ln = lanthanide) + O_2/O_3
	Ln_2O_3, $LnSi_xO_y$, $LnAlO_3$	Dielectric capacitor layers in DRAMs	Metal alkoxides, (*e.g.* $[M(OR)_4]$ (M = Si, Ti, Zr, Hf), $[M(OR)_5]$ (M = Ta, Nb) + O_2/O_3
	SiO_2, Ta_2O_5, Nb_2O_5	Dielectric capacitor layers in DRAMs	
		Optical coatings	Metal alkylamides $[M(NR_2)_4]$ (M = Ti, Zr, Hf) + O_2/O_3
			Organometallics (*e.g.* $[Cp_2MMe_2]$, $[(RCp)_2MMe_2]$ (M = Zr, Hf) + O_2/O_3
			$[LaCp_3]$, $[Ln(RCp)_3] + O_2/O_3$
Ferroelectric oxides	$SrTiO_3$, $(Ba,Sr)TiO_3$, $Pb(Zr,Ti)O_3$, $SrBi_2(Ta_xNb_{1-x})_2O_9$, $Bi_4Ti_3O_{12}$, $Pb(Sc,Ta)O_3$, $Pb(Mg,Nb)O_3$	DRAMs, NVFERAM , computer memories, infrared detectors, microelectromechanical devices, transducers, ceramic capacitors,	Metal-β-diketonates ($[Ba(thd)_2]$, $[(Sr(thd)_2]$, $[Ti(OPr^i)_2(thd)_2]$, $[Bi(thd)_3]$
			$[Pb(thd)_2]$, $[Sc(thd)_3]$, $[Mg(thd)_2] + O_2$
			Metal alkoxides ($[Bi(OR)_3]$, $[Ta(OR)_5]$, $[Nb(OR)_5]) + O_2$
Ferrites	$(Ni,Zn)Fe_2O_4$, $(Mn,Zn)Fe_2O_4$	Recording media, high frequency read heads	Metal-β-diketonates ($[Ni(thd)_2]$, $[Zn(thd)_2]$, $[Mn(thd)_2]$, $[Fe(thd)_3]) + O_2$
Superconducting oxides	$YBa_2Cu_2O_{7-x}$, Bi-Sr-Ca-Cu-O	Josephson junctions, bolometers, SQUIDS	Metal-β-diketonates ($[Y(thd)_3]$, $[Ba(thd)_2]$, $[Sr(thd)_2]$, $[Cu(thd)_2]$, $[Ca(thd)_2]) + O_2$
Conducting oxides	$(La,Sr)CoO_3$, $(La,Mn)O_3$ RuO_2, $SrRuO_3$	Ferroelectric capacitor electrodes	Metal-β-diketonates + O_2
			$[Ru_3(CO)_{12}]$, $[Ru(\beta\text{-dik})_3]$, $[Ru(RCp)_2]$ (R = H, Et)
Low-emissivity and conducting oxides	F-doped SnO_2	Architectural coatings on flat glass (solar control, anti-reflective), display coatings on glass	$[SnCl_4]/[NH_4F]/O_2$
	Sn-doped In_2O_3		$[InCl_3]/[SnCl_4]/O_2$,$[In(thd)_3]/[Bu_2Sn$ (acetate)]/O_2, $[In(acac)_3]/[Sn(acac)_2]/O_2$
Electrochromic and photochromic oxides	WO_3	Architectural coatings on flat glass (displays)	$[WCl_6]/O_2$, $[W(CO)_6]/O_2$
	MoO_3		$[Mo(CO)_6]/O_2$

(*Continued*)

Table 1.3 (*continued*).

General class of material	*Specific material*	*Applications*	*Typical CVD precursors*
Thermochromic oxides	VO_2	Architectural coatings on flat glass	$[VCl_4]/O_2$, $[VOCl_3]/O_2$
Self-cleaning coatings	TiO_2	Architectural coatings on flat glass	$[TiCl_4]/[Ti(OPr^i)_4]/O_2$
Garnets	$Y_3Fe_5O_{12}$	Microwave elements, magneto-optic recording	Metal-β-diketonates + oxygen
Elemental semiconductors	Si	Microelectronic devices	$[SiH_4]$, $[Si_2H_6]$, $[SiH_xCl_{4-x}]$ ($x = 0$–3)
	Doped-Si		$[SiH_4]/[PH_3]/[AsH_3]/[B_2H_6]$
	Ge		$[GeH_4]$
	Diamond and diamond-like carbon	Semiconductor devices	$[C_nH_{2n+2}]$
III-V Compound Semiconductors	GaAs	Solar cells, LEDs	Gp. III trialkyls, $[R_3M]$ (M = Ga, In, Al; R = Me, Et) + Group V trihydrides ($[AsH_3]$, $[PH_3]$, $[NH_3]$ or organometallics ($[Bu^tAsH_2]$, $[Bu^tPH_2]$, $[R_3Sb]$)
	GaAs/AlGaAs	Heterostructure lasers, solar cells, HEMTS, HBTs, FETs	
	GaP	Red LED, photocathodes	
	GaAsP, InGaP	Red LEDs	
	AlGaInP	Yellow/green LED	
	GaN	Blue LED	
	InGaN	Green LED	
	InGaP/AlGaInP	Red laser pointers	
	InP	Gunn diodes, radar devices	
	InP/InGaAs	Detectors in optical fibre technology	
	InGaAsP	Emitters in optical fibre technology	
	GaSb/AlGaSb	Thermal imaging devices, environmental sensors	
II-VI compound semiconductors	ZnS	Blue phosphors, TFELs	Gp. II dialkyls, $[R_2M]$ (M = Zn, Cd; R = Me) + Gp VI dihydrides, $[H_2Se]$, $[H_2S]$ or Gp VI dialkyls, $[Et_2Se]$, $[Et_2S]$, $[Et_2Te]$, $[Pr^i{}_2Te]$
	ZnSe, ZnSSe, ZnMgSSe	Blue/green LEDs and lasers	
	ZnCdS, CdS/CdTe	Solar cells	
	CdTe, CdHgTe	Infrared detector, thermal imaging systems	
Metals	Al	Interconnects in microelectronic devices, metallized polymers, gas	$[Bu^i_3Al]$, $[AlH_3(NR_3)]$

		diffusion barriers, optical coatings, adhesion aid	
	W	Metallization in transistors, interconnects in ICs, wear and erosion protection	$[WF_6]$, $[WCl_6]$,/H_2; $[W(CO)_6]$; W-alkyls
	Cu	Interconnects in ICs	Cu(II) β-diketonates/H_2; [(hfac)Cu(I)L] (L = $[PMe_3]$, [1,5-COD], alkyne, VTMS)/H_2
	Au, Ag	Metallization in ULSI	Me_2Au(β-diketonate)]; [Ag(β-diketonate)]
	Pt, Pd, Ni	Metal contacts in microelectronic devices, catalysts, protective and decorative coatings	$[Pt(acac)_2]$, $[PtMe_3]$; $[(1,5\text{-COD})PtMe_2]$; $[Pd(allyl)_2]$; [CpPd(allyl)]; $[Ni(CO)_4]$; $[NiCp_2]$; $[Ni(MeCp)_2]$
	Ti	Adhesion layers, metal foils, corrosion resistant coatings	$[TiI_4]$, $[TiBr_4]/H_2$
	Cr	Corrosion protection	$[CrF_2]$, $[CrCl_2]$, $[Cr(CO)_6]$, $[CrPh_2]/H_2$
	Mo	IC contact and gate metallization, wear resistant coatings, infrared reflector, laser mirror coating	$[MoF_5]$, $[MoCl_5]$, $[Mo(CO)_6]$
	Ru	IC contact and gate metallization, diffusion barriers	$[Ru_3(CO)_{12}]$, $[RuCp_2]$, $[Ru(acac)_2]/H_2$
	Ta	Capacitors, resistors, corrosion resistant coatings	$[TaCl_5]$, $[TaF_5]$, $[Ta(CO)_5]/H_2$
Metal nitrides	AlN	Surface acoustic wave devices, packaging material in microelectronic devices	$[AlBr_3]/[NH_3]$, $[AlMe_3/NH_3]$; $[Al(NMe_2)_3]/[NH_3]$; $[AlMe_3(NH_3)]$ adduct
	Si_3N_4	Chemical passivation, encapsulation of silicon bipolar and MOS devices	$[SiH_4]/[NH_3]$; $[Si_2Cl_6]/[NH_3]$; $[Si(NMe_2)_{4-n}H_n]$
	TiN	Wear-resistant and friction reducing coatings, transparent optical films, energy efficient windows, decorative coatings, low resistant contacts, diffusion barriers, and gate electrodes in microelectronic devices	$[TiCl_4]/[NH_3]$, $[TiI_4]/[NH_3]$; $[Ti(NR_2)_4]/[NH_3]$
	ZrN, HfN	Hard coatings for machine tools, diffusion barriers and gate electrodes in microelectronics	$[M(NR_2)_4]/[NH_3]$; $[M(NEt_2)_4]/[Me_2NNH_2]$; $[M(NR_2)_4/N_2]$(plasma-assisted)
	TaN, NbN	Diffusion barriers for Cu in ICs; gate electrodes	$[TaCl_5]/[NH_3]$, $[TaBr_5]/[NH_3]$; $[Ta(NMe_2)_5]/[NH_3]$, $[Ta(NEt_2)_5]/[NH_3]$; $[Ta(NEt_2)_3(N\text{-}Bu^t)]/[NH_3]$; $[Ta(NEt_2)_3(NCMe_2Et)]/[NH_3]$

(*Continued*)

Table 1.3 (*continued*).

General class of material	*Specific material*	*Applications*	*Typical CVD precursors*
			$[NbCl_5]/[NH_3]$; $[NbCl_5]/[Me_2NNH_2]$; $[Nb(NR_2)_5]/[NH_3]$, $[Nb(NR_2)_4]/[NH_3]$
	WN	Diffusion barriers, gate electrodes in microelectronic devices	$[WCl_6]/[NH_3]$, $[WF_6]/[NH_3]$; $[W(CO)_6]/[NH_3]$; $[W(NBu^t)_2(NR_2)_2]/[NH_3]$; $[(RN)WCl_4(NCR)]/[NH_3]$; $[W_2(NMe_2)_6]/[NH_3]$
	MoN		$[MoF_6]/[NH_3]$, $[Mo(CO)_6]/[NH_3]$; $[Mo(NMe_2)_4]/[NH_3]$; $[Mo(NBu^t)_2(NMe_2)_2]/[NH_3]$
Metal carbides	TiC	Hard coating for cutting, milling, forming and stamping tools	$[TiCl_4]/[CH_4]$; $[Cp_2TiCl_2]/[H_2]$
	ZrC	Coating for nuclear fuel particles	$[ZrCl_4]$, $[ZrBr_4]/[CH_4]$ or $[C_3H_{11}]$
	HfC	Oxidation-resistant coating for composites, coating for superalloys	$[HfCl_4]/[CH_4]$
	Cr_7C_3, Cr_3C_2	Corrosion- and wear-resistant coatings	$[CrCl_3]$/n-butane; $[Cr(C_6H_5\text{-i-}Pr)_2]$; $[CrBu^t{}_2]$
	WC, W_2C, W_3C	Tool coatings, catalysts	$[WF_6]$/cyclopropane; $[WCl_6]/[CH_4]$
	V-carbide	Wear- and corrosion-resistant coatings	$[VCl_4]/[CH_4]$; $[VCp_2]$
	Ta, Nb-carbide	Protective coatings	$[TaCl_5]/[MeCl]/[H_2]$; $[NbCl_5]/[CCl_4]/[H_2]$
	SiC	Blue LEDs, heat sinks, protective coatings	$[MeSiCl_3]/[H_2]$
	GeC	Optical coatings	$[C_nH_{2n+2}]/[GeH_4]$

Abbreviations: β-dik=β-diketonate, acac=acetylacetonate, thd = tetramethylheptanedionate, hfac=hexa fluoroacetylacetonate (Ch. 8, Table 8.2), $C_p=C_5H_5$, $RC_p=RC_5H_4$, 1,5-COD=1,5 cyclooctadiene.

significantly influenced by CVD process parameters such as growth temperature, partial pressures of gaseous species and the total pressure of the system. A detailed description of how such parameters affect the microstructure of CVD-grown layers is not yet available, but a few useful reviews describe the current state of understanding.[86–89] Three main types of morphology are briefly discussed below. Various analytical techniques are used to determine layer morphology. Scanning electron microscopy (SEM) and atomic force microscopy (AFM) give information about crystallinity to the sub-micrometer level, whilst crystalline orientation can be determined by X-ray diffraction (XRD), which also allows the observations of the transition when amorphous layers, with no features in XRD, crystallize to give clearly defined X-ray diffraction peaks.

1.7.1.1 Epitaxial Layers

Epitaxial layers are single crystal films grown by lattice matching the crystalline spacings of the film and underlying substrate. To achieve this it is important that the substrate is free from defects and surface contamination. Also for epitaxy, low growth rates are required so that surface diffusion is fast relative to the arrival of new growth initiating species on the surface. This allows adsorbed species to diffuse to step growth sites and form a layer that replicates the underlying substrate. Growth at high temperatures (typically $> 700\ ^{\circ}C$) is generally required to promote epitaxy since this increases the desorption of impurities as well as the surface mobility of adsorbed precursor species. Growth on a substrate of the same material is called homoepitaxy and growth on a different material, but with very similar crystal structure, is known as heteroepitaxy. A good review on the epitaxial growth of silicon by CVD has been published,[28] and the importance of epitaxial growth of compound semiconductors is illustrated in Chapter 6 of this book.

1.7.1.2 Amorphous Layers

The formation of amorphous films is promoted by very high growth rates and low substrate temperatures, where the arrival of film precursors is much more rapid than the diffusion of surface species. However, care has to be taken not to leave films grown in the amorphous state in a hot reactor for any length of time since this can lead to annealing and crystallization.

1.7.1.3 Polycrystalline Layers

Polycrystalline layers are often deposited at intermediate temperatures and growth rates between those used for growth of single crystal and amorphous films. Polycrystalline growth is facilitated by polycrystalline surfaces where nucleation occurs at many different surface sites, leading to growth of islands that coalesce to form a polycrystalline layer. The control of the size and nature of the crystallites is important in determining the properties of CVD films.

In Figure 1.17, the SEM data for an amorphous data film of Hf-silicate are compared to the SEM data for a polycrystalline film of HfO_2. The columnar microstructure of the oxide film is in marked contrast to the featureless structure of the Hf-silicate film. The transition from an amorphous to a polycrystalline phase is illustrated by XRD data for a HfO_2 film deposited at various substrate temperatures (Figure 1.18), from which it can be seen that the crystallinity of the material is a strong function of growth temperature, with the polycrystalline monoclinic phase forming at 450 °C and above.

1.7.2 Layer Properties

The aim of depositing a film by CVD is to obtain a functional material with specific mechanical, electrical, magnetic, optical or chemical properties, or a combination of several of these properties.

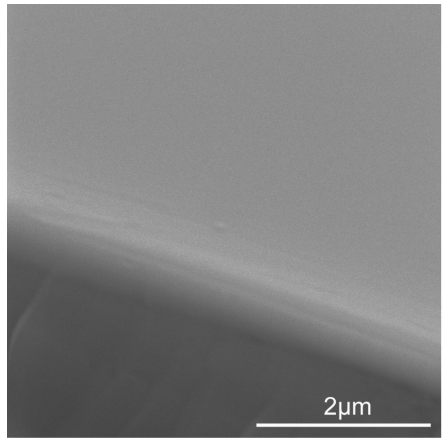

(a)

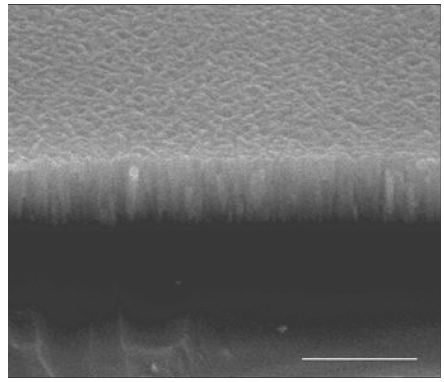

(b)

Figure 1.17 SEM data for (*a*) an amorphous HF-silicate film and (*b*) a polycrystalline HfO_2 film.

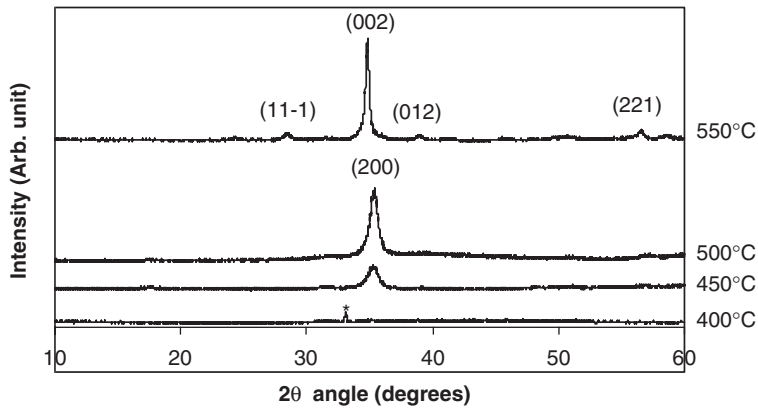

Figure 1.18 Variation of crystallinity of HfO_2 grown by MOCVD with growth temperature.

Layer properties can be strongly influenced by several film characteristics common to all CVD-grown layers.

1.7.2.1 Layer Thickness and Density

The thickness of layers deposited by CVD can vary over a wide range, from single atomic layers (*e.g.* in ALD), through a few nanometres in, for example, multi-quantum well structures, to hundreds of nanometres for optical and semiconductor applications, and even to greater than 100 μm for some applications such as wear resistant coatings. Layer thickness is dependent on both the CVD technique employed and the range of deposition parameters.

Thick films result from high growth rates often associated with high temperatures and pressures of many thermal CVD and PECVD processes, whilst thin films are obtained from the low growth rates and nano-scale control that are a feature of ALD and CBE techniques. Layer thickness is generally measured after deposition by optical techniques (*e.g.* interferometry and ellipsometry), scattering techniques (*e.g.* Rutherford scattering and β back scattering), electromechanical profilometry or microscopy (using an optical microscope or scanning electron microscope after layer sectioning). Simple weighing of the substrate using an accurate microbalance before and after film deposition can also be used to measure layer thickness, provided the density of the layer is known. The measure of weight variation as a function of time using a quartz crystal oscillator, or by deposition on a substrate suspended from the arm of a microbalance, allows the *in situ* monitoring of layer growth.

Film density is a measure of the quality and potential functionality of the film, with low density films indicative of high porosity and the incorporation of impurities in the crystal lattice, possibly due to incomplete decomposition of the precursor, as often observed in films grown at low temperature (*e.g.* by ALD). Film density generally increases as the growth temperature increases, or by high temperature annealing of the film, and the refractive index of the film can give a measure of film density, with dense films having high refractive indices.

1.7.2.2 Layer Adhesion

For any practical use, it is essential that a CVD film adheres well to the substrate. However, the factors that influence film adhesion are not totally understood, although it is generally accepted that to promote good film adhesion it is important that the substrate surface is thoroughly cleaned before film growth. The reason for this is that impurities on the surface can inhibit deposition of a coating and can also significantly affect the mode and amount of nucleation of depositing material. The measurement of adhesion is still very much based on empiricism, as it is difficult to quantitatively model the forces governing adhesion. Consequently, for example, qualitative assessment of how well a film is adhering to a substrate is made by the rather unsophisticated technique of the "scratch test"[90] and the even less sophisticated "Scotch tape test."[91] The real test, though, of any film adhesion comes when the layer is put to a practical application. A good review of the qualities necessary in effective protective coatings is available.[92]

1.7.2.3 Layer Composition and Purity

Layer composition and purity are vital factors in determining the functionality of a CVD film. Layer composition can be measured by several techniques such as Auger electron spectroscopy (AES), X-ray photoelectron spectroscopy (XPS), Rutherford back scattering (RBS), time-of-flight elastic recoil spectrometry (TOF-ERDA), energy or wavelength dispersive X-ray analysis (EDX or WDX) and secondary ion or secondary neutral mass spectrometry (SIMS or SNMS). The first five

of these techniques can determine bulk stoichiometry of a layer and impurities, such as carbon and nitrogen, down to levels of about 1 at.%. SIMS is a much more sensitive technique, capable of detecting impurities in the film down to the ppm, or even ppb, levels, although quantitative analysis needs careful calibration samples to be made. SNMS, on the other hand, can measure from the high atomic % down to ppm much more readily.

The reason that it is important to be able to determine layer composition at very low levels is that even very small traces of an impurity species can dramatically affect layer characteristics. This is true for layers that are grown for optical, mechanical, chemical and magnetic applications, but it is particularly so for materials that are deposited with specific electrical properties in mind. This is illustrated in the next section, which considers the electrical characteristics of compound semiconductor layers.

A rather specialized technique used to investigate the thickness, composition and crystallinity of thin films is medium energy ion scattering (MEIS). This involves bombarding the film with energetic He^+ ions (~ 200 keV), and then analysing the energy of the ions scattered from the film. Owing to the inelastic scattering that the He^+ ions undergo as a function of depth below the sample surface, the energy distribution gives an effective depth profile of the target atoms. MEIS also provides valuable information on the extent of interaction between the film and the substrate, particularly valuable in assessing the stability of dielectric oxide films on Si for CMOS and DRAM applications, with film crystallization often leading to an increased film–substrate interaction.

The method used for determining the properties and functionality of a thin film clearly depends on the specific application. However, due to the increasing importance in microelectronics of thin films grown by CVD, some methods used for the characterization of two types of film from this area of technology are discussed below.

1.7.2.4 Electrical Characterization of Compound Semiconductor Films

The principal electrical parameters used to characterize III–V or II–VI compound semiconductor materials are the carrier concentration, n (*i.e.* the number of charge carriers per cm^3) and the carrier mobility, which is a measure of the ease with which the carriers can move under the influence of an electrical field. The mobility of the charge carriers in a semiconductor is a more complicated function of temperature than the conductivity of a metal because, besides the temperature dependent scattering processes found in metals the actual number of carriers (n) and their energy distribution are temperature dependent.

The carrier concentration and carrier mobility in a semiconductor can be determined from the conductivity of the film, which is derived from resistivity measurements on the layer using the four-point probe method[93] and Hall measurements. The measured value of n represents the *net* value of residual charge carriers and is thus a balance between the total concentration of ionized donor (N_D) and acceptor impurities (N_A). Once the carrier mobility has been determined, it is possible to determine the concentrations of ionized donor and acceptor impurities and the ratio N_A/N_D (the compensation ratio) is often used as an indication of layer purity. For n-type material the residual electron concentration is often expressed as n, although the term $(N_D - N_A)$ is more accurate, and residual hole density can be expressed as p or $(N_A - N_D)$.

High purity compound semiconductor material will have a low residual carrier concentration and a correspondingly high carrier mobility. For instance a good quality GaAs layer might have a residual carrier concentration (n) of $1 \times 10^{14}\,cm^{-3}$ and a mobility (μ) at 77 K of $130\,000\,cm^2\,V^{-1}\,s^{-1}$, with the material having a relatively low level of donor impurities ($N_D = 1.4 \times 10^{14}\,cm^{-3}$) and an even lower level of acceptor impurities ($N_A = 0.4 \times 10^{14}\,cm^{-3}$). The low compensation ratio (N_A/N_D) of 0.28 shows that the film is high purity. By contrast, a low purity sample of GaAs may still have a low *residual* carrier concentration (n) of, for example, $1 \times 10^{14}\,cm^{-3}$, but a low electron

mobility (*e.g.* 26 500 $cm^2 V^{-1} s^{-1}$) at 77 K reflects the low purity of the sample. This is due to the presence of high levels of donor *and* acceptor impurities ($N_D = 2 \times 10^{15}\,cm^{-3}$; $N_A = 1.9 \times 10^{15}\,cm^{-3}$), which lead to the very low charge mobility because of impurity scattering. In this case, the compensation ratio of 0.96 is high.

The dramatic effect of impurities on layer properties can be seen by relating carrier concentrations to the level of impurity incorporated in the layer. For example, a GaAs layer with a carrier mobility of 130 000 $cm^2 V^{-1} s^{-1}$ and a carrier concentration of $1 \times 10^{14}\,cm^{-3}$ has one carrier atom per 2.167×10^8 gallium atoms, or 4×10^{-7} mol.% of carriers.

1.7.2.5 Electrical Characterization of Dielectric Thin Films

A detailed review covering the physics of metal-oxide semiconductors has been published.[94] However, in view of the great importance of dielectric films in microelectronics applications,[95] [see, for example, Chapters 4 (Section 4.5.3) and 8 (Section 8.3)] it may be useful to briefly describe how the films are frequently characterized.

For dielectric thin films, key parameters are the permittivity or dielectric constant (κ) and leakage current. For insulating gate oxides (*e.g.* SiO_2, HfO_2) deposited on a Si substrate, high frequency capacitance–voltage (*C-V*) data on a metal/oxide/semiconductor capacitor (MOSC) can be used to determine film quality.[96] Figure 1.19 shows the high-frequency *C-V* data for a [Al/HfO_2/SiO_2/p-Si] MOSC structure, before and after annealing. The HfO_2 dielectric layer was deposited by ALD at 360 °C using alternating pulses of [Hf(mmp)$_4$] (mmp = $OCMe_2CH_2OMe$) (Chapter 8, Section 8.3.1.2) and water.[97]

The *C-V* curves show features characteristic of a well-insulating dielectric material with a high capacitance *accumulation region* at negative bias voltages, a *depletion region* of decreasing capacitance, and a low capacitance *inversion region* at positive biases. The capacitance of the MOSC structure is a series combination of metal oxide capacitance and the Si semiconductor depletion layer capacitance. At negative bias voltages, the majority charge carriers (holes) in the p-type Si are attracted towards the gate oxide. The holes accumulate at the HfO_2/Si interface and

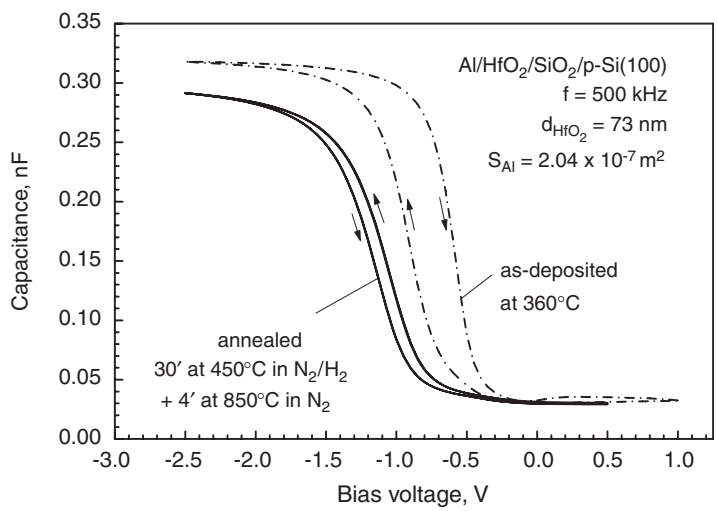

Figure 1.19 High-frequency (500 kHz) *C-V* data for a [Al/HfO_2/SiO_2/p-Si] MOS structure fabricated by ALD using [Hf(mmp)$_4$] and H_2O. (Reprinted with permission from ref. 97. Copyright 2003, American Chemical Society.)

there is no depletion region. As a result, the measured capacitance is close to the HfO_2 film capacitance and the effective dielectric constant, or permittivity, (κ) of the HfO_2 film is given by Equation (1.3):

$$\kappa = C_{ox} d / \varepsilon_0 A \tag{1.3}$$

where C_{ox} = capacitance value in accumulation region, d = oxide layer thickness, A = area of gate contact (in this case $1.96 \times 10^{-7}\,m^2$) and ε_0 = permittivity of free space ($8.854 \times 10^{-12}\,F\,m^{-1}$).

As the gate voltage becomes more positive, the positive gate electrostatically repels the holes away from the HfO_2/Si interface. A depletion zone penetrates more deeply into the Si semiconductor and the depletion capacitance becomes smaller, reducing the overall capacitance of the MOSC stack. The depletion layer broadens, until there is an accumulation of minority charge carriers (electrons) at the Si/insulating oxide interface. The accumulated minority carrier layer is called the inversion layer, because the original polarity of the surface has now become inverted. In equilibrium conditions, the minority carriers in the inversion layer inhibit further penetration of the electric field in the semiconductor, leading to the minimum capacitance values in the *C-V* curve.

The amount of hysteresis in the *C-V* curve during a backwards and forwards voltage sweep across the capacitor provides information about the amount of mobile ionic charge (*e.g.* H^+ ions) and/or slow states in the dielectric oxide film. The flatband voltage shift (ΔV_{FB}) is the difference in bias voltage measured at the flat band capacitance in the depletion region in the *C-V* curve from the flatband voltage calculated for the ideal case ($\sim$–0.9 to -1.0 V), and is a measure of interface quality, indicating the amount and nature of fixed charge at the dielectric/Si interface. The *C-V* data for the [Al/HfO_2/SiO_2/p-Si] structure shown in Figure 1.19 clearly show that the quality of the HfO_2 film improves after annealing, with a marked decrease in hysteresis and a reduced flatband voltage shift, indicating a reduction in mobile ions and interface fixed charge.

The *C-V* data for an n-type MOSC such as [Al/HfO_2/SiO_2/n-Si], in which the majority charge carriers in the Si are electrons, are essentially a mirror image (in the *y*-axis) of the p-type MOSC curve shape, with the accumulation region occurring at positive polarities and the inversion region at negative polarities.

When comparing different dielectric materials, and especially high-κ dielectric oxide films used in gate dielectric and capacitor applications (Chapter 8, Section 8.3), the films are often characterized by quoting the "equivalent oxide thickness" (EOT), which is the theoretical thickness of SiO_2 that would provide the same capacitance density as the alternative high-κ dielectric (ignoring the effect of leakage current and reliability).

Current–voltage (*I-V*) data obtained on MOSC structures are also frequently used to assess the quality of an insulating dielectric film. *I-V* data give a measure of the leakage of current through the film at a particular applied voltage and they are critically dependent on film thickness, polarity of applied voltage, gate electrode material and the type and nature of defects in the film, with thin films generally giving higher leakage currents than thick films of the same material. As an approximate guide, leakage current densities for a thin film (*e.g.* $\sim$5 nm) of a high quality dielectric oxide are generally below $\sim 5 \times 10^{-5}$ A cm^{-2}. For instance, Figure 1.20 shows a plot of leakage current density (J) against electric field (E_{ox}) for a series of HfO_2 films grown by liquid injection MOCVD and ALD using [$(MeCp)_2HfMe(OR)$] (OR = OPr^i, mmp).[98] The data show that all films showed good electrical integrity ($< 2 \times 10^{-5}\,A\,cm^{-2}$) at 1 MV cm^{-1}, although it must be noted that the films grown by ALD are much thinner (1.7 and 9.6 nm) than those grown by MOCVD (76 and 102 nm), indicating that they are better insulators. At higher electric fields ($\sim 2.5\,MV\,cm^{-1}$) the leakage current density of three of the films rose considerably to $\sim 1 \times 10^{-4}$ to $5 \times 10^{-3}\,A\,cm^{-2}$, indicating some breakdown in the integrity of these HfO_2 films.

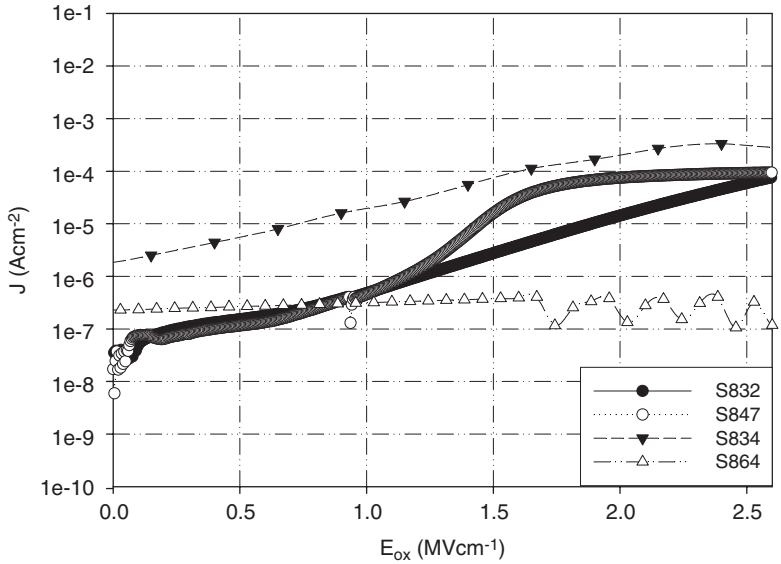

Figure 1.20 Leakage current density (J) versus electric field (E_{ox}) for HfO_2 films deposited by MOCVD (●,○) (film thicknesses 76 and 102 nm) and ALD (▼, △) (film thicknesses 1.7 and 9.6 nm). (After ref. 98, Copyright Wiley-VCH Verlag GmbH & Co. KGaA, 2007. Reproduced with permission.)

1.8 Postscript

Although it is impossible in a chapter of this length to give a comprehensive overview, it is hoped that this brief description of some of the main elements of CVD gives a flavour of the complex interweaving threads associated with the technology. For more detailed descriptions of the many various aspects of CVD processes read on!

References

1. G. B. Stringfellow, *Chapter 1 in Organometallic Vapor Phase Epitaxy*, Academic Press, New York, 1989.
2. M. L. Hitchman and K. F. Jensen, in *Chemical Vapor Deposition*, eds. M. L. Hitchman and K. F. Jensen, Academic Press, New York, 1989, Chapter 1.
3. T. T. Kodas and M. J. Hampden-Smith, *Chapter 1 in The Chemistry of Metal CVD*, VCH, Weinheim, 1994.
4. A. C. Jones and P. O'Brien, in *CVD of Compound Semiconductors*, VCH, Weinheim, 1997, and references therein.
5. R. L. Moon and Y.-M. Houng, in *Chemical Vapor Deposition*, Eds. M.L. Hitchman and K.F. Jensen, Academic Press, New York, 1989, Chapter 6.
6. E. M. Sherwood and J. M. Blocher, *J. Metals*, 1965, **17**, 594.
7. C. F. Powell, J. H. Oxley and J. M. Blocher, *Vapour Deposition*, The Electrochemical Society, Pennington NJ, 1966.
8. J. F. Gallie, *Petroleum Refiner*, 1944, **23**, 176.
9. W. E. Sawyer and A. Mann, *US Patent 229,335* (1880).
10. J. W. Aylsworth, *US Patent, 553,296* (1896).
11. A. de Lodyguine, *US Patent 575,002* (1897).

12. F. Wöhler and L. Uslar, *Lieb. Ann.*, 1855, **94**, 255.
13. L. Mond, C. Langer and F. Quincke, *J. Chem. Soc.*, 1890, **57**, 749.
14. L. Mond, *U.S. Patent, 455,230*, 1891.
15. R. Mond, *Chem. Ind.*, 1930, **49T**, 371.
16. J. N. Pring and W. Fielding, *J. Chem. Soc.*, 1909, **95**, 1497.
17. R. Hoelbling, *Z. Angew.Chem.*, 1927, **40**, 655.
18. G. K. Teal, J. R. Fisher and A. W. Treptow, *J. Appl. Phys.*, 1946, **17**, 879.
19. K. H. Storks and G. K. Teal, *US Patent 2,441,603* (1948).
20. M. J. Cook, R. A. Heinecke, R. C. Stern and J. W. Maes, *Solid State Technol.*, 1982, **25**(12), 62.
21. M. L. Green, R. A. Levy, R. G. Nuzzo and E. Coleman, *Thin Solid Films*, 1984, **114**, 367.
22. T. P. Whaley and V. Norman, *US Patent 3,209,326* (1965).
23. D. R. Carley and J. H. Dunn, *US Patent 3,375,129* (1968).
24. D. L. Schmidt and R. Hellmann, *US patent 3,462,288* (1969).
25. W. L. Gladfelter, D. C. Boyd and K. F. Jensen, *Chem. Mater.*, 1989, **1**, 339.
26. Pilkington Brothers Ltd., *Proceedings of The Royal Society of London Series A-Mathematical And Physical Sciences*, 1969, **314**, 1.
27. R. Glang and B. W. Kippenham, *IBM J. Res. Devel.*, 1960, 299.
28. B. S. Meyerson, in *Chemical Vapor Deposition*, eds. M. L. Hitchman and K. F. Jensen, Academic Press, New York, 1989, Chapter 5.
29. R. Didchenko, J. D. Alix and R. H. Toeniskoettler, *J. Inorg. Chem.*, 1960, **4**, 35.
30. B. Harrison and E. H. Tomkins, *Inorg. Chem.*, 1962, **1**, 951.
31. Monsanto Co. *US Patent Applications 113,108 and 129,919* (1961).
32. Monsanto Co. *UK Patent 1,011,979* (1965).
33. H. M. Manasevit, *Appl. Phys. Lett.*, 1968, **12**, 156.
34. H. M. Manasevit, *U.S. Patent, 4,368,098C*, 1983.
35. P. Rhai Choudry, *J. Electrochem. Soc.*, 1969, **116**, 1745.
36. H. M. Manasevit, *J. Electrochem. Soc.*, 1971, **118**, 647.
37. H. M. Manasevit and W. I. Simpson, *J. Electrochem. Soc.*, 1971, **118**, C291.
38. H. M. Manasevit and W. I. Simpson, *J. Electrochem. Soc.*, 1973, **120**, 135.
39. H. M. Manasevit and W. I. Simpson, *J. Electrochem. Soc.*, 1971, **118**, 1864.
40. Y. Seki, K. Tanno, K. Iida and E. Ichiki, *J. Electrochem. Soc.*, 1975, **122**, 1108.
41. S. J. Bass, *J. Crystal Growth*, 1975, **31**, 172.
42. R. D. Dupuis and P. D. Dapkus, *Appl. Phys. Lett.*, 1977, **31**, 466.
43. S. Nakamura, T. Mukai and M. Senoh, *Appl. Phys. Lett.*, 1994, **64**, 1687.
44. A. D. Berry, D. K. Gaskill, R. T. Holm, E. J. Cukauskas, R. Kaplan and R. L. Henry, *Appl. Phys. Lett.*, 1988, **52**, 1743.
45. *High Temperature Superconductors: Fundamental Properties and Novel Materials Processing*, eds. D. Christen, J. Narayan and L. Scneemeyer, Material Research Society Symposium Proceeding, 1990, Vol. **169**, and references therein.
46. G. J. M. Dormans, P. J. van Veldhoven and M. de Keijser, *J Crystal Growth*, 1992, **123**, 537.
47. A. C. Jones, *J. Mater. Chem.*, 2002, **12**, 2576.
48. T. Suntola and J. Antson, *US Patent 4,058,430* (1977).
49. T. Suntola, *Mater. Sci. Rep.*, 1989, **4**, 261.
50. T. Suntola, J. Antson, A. Pakkala and S. Lindfors, *SID 80 Digest*, 1980, **11**, 108.
51. M. Leskelä and L. Niinistö, Electroluminescence, *Proc. 6th Int. Workshop on Electroluminescence*, Cino Puntos Press, El-Paso, 1992, pp. 249–246.
52. P. O'Brien, in *Inorganic Materials*, Chapter 9, eds. D.W. Bruce and D. O'Hare, Wiley, New York, 1992, p. 500.
53. M. R. Leys, *Chemtronics*, 1987, **2**, 155.
54. R. H. Reep and S. K. Ghandi, *J. Crystal Growth*, 1983, **61**, 499.

55. D. W. Hess and D. B. Graves, in *Chemical Vapor Deposition*, Eds. M. L. Hitchman and K. F. Jensen, Academic Press, New York, 1989, Chapter 7, and refs. therein.
56. V. R. McCrary and V. M. Donnelly, in *Chemical Vapor Deposition*, eds. M. L. Hitchman and K. F. Jensen, Academic Press, New York, 1989, Chapter 8, and refs. therein.
57. M. Leskelä and M. Ritala, in *Handbook of Thin Film Materials*, ed. H.S. Nalwa, Academic Press, 2002, Vol. **1**, p. 103.
58. W. T. Tsang, *J. Crystal Growth*, 1990, **105**, 1.
59. W. T. Tsang, *J. Electron. Mater.*, 1986, **15**, 235.
60. G. J. Davies and D. A. Andrews, *Chemtronics*, 1988, **3**, 3.
61. T. F. Keuch and E. Veuhoff, *J. Crystal Growth*, 1984, **68**, 148.
62. A. C. Jones, H. C. Aspinall, P. R. Chalker, R. J. Potter, T. D. Manning, Y. F. Loo, R. O'Kane, J. M. Gaskell and L. M. Smith, *Chem. Vap. Deposition*, 2006, **12**, 83.
63. M. Fulem K. Růžiča, E. Hulicius, T. Šimeček, K. Melichar, J. Pangrác, S. A. Rushworth and L. M. Smith, *J. Crystal Growth*, 2003, **248**, 99.
64. C. L. Griffiths, A. Stafford, S. J. C. Irvine, N. Maung, A. C. Jones, L. M. Smith and S. A. Rushworth, *Appl. Phys. Lett.*, 1996, **68**, 194.
65. O. Kayser, *Chemtronics*, 1988, **3**, 90.
66. S. A. Rushworth, L. M. Smith, A. J. Kingsley, R. Odedra, R. Nickson and P. Hughes, *Microelectronics and Reliability*, 2005, **45**, 1000.
67. S. Duffy, P. F. Nolan, S. A. Rushworth, A. B. Leese and A. C. Jones, *Adv. Mater. Opt. and Electron.*, 1997, **7**, 233.
68. A. C. Jones, *Chemtronics*, 1989, **4**, 15.
69. S. Fujita, Y. Uemoto, S. Araki, M. Imaizumi, Y. Takeda and A. Sarasaki, *Jpn. J. Appl. Phys.*, 1988, **27**, 1151.
70. R. A. Smith, in *Semiconductors* (Cambridge University Press, Cambridge, 1978) Chapter 3.
71. A. C. Jones, G. Wales, P. J. Wright and P. E. Oliver, *Chemtronics*, 1987, **2**, 83.
72. T. Nakanisi, T. Udagawa, A. Tanaka and K. Kamei, *J. Crystal Growth*, 1981, **55**, 255.
73. A. C. Jones and P. O'Brien, *Chapter 2 in CVD of Compound Semiconductors*, VCH, Weinheim, 1997.
74. A. A. Efremov, V. A. Federov and E. E. Grinberg, translated from *Vysokchiste Veschestra*, No. 3, May-June 1998, pp 5-43, Plenum Publishing Corp. 1989.
75. E. E. Grinberg and A. A. Efremov, *Electron. Tekh. Ser. Mat.*, 1975, **7**, 62.
76. V. G. Makarenko, V. A. Federov and A. A. Efremov, *Electron. Tekh. Ser. Mat.*, 1974, **11**, 71.
77. A. A. Efremov, E. E. Grinberg, Yu M. Fetisov, USSR Pat. 546,617, *Byull. Izobrett.*, 1977, **6**.
78. H. Kodakura, K. Sawara and T. Yako, *U. K. Pat. Application. GB 2,183,651(A)*, (1987).
79. A. C. Jones, D. J. Cole-Hamilton, A. K. Holliday and M. Munir Ahmad, *J. Chem. Soc., Dalton Trans.*, 1983, 1047.
80. A. H. Moore, M. D. Scott, J. I. Davies, D. C. Bradley, M. M. Faktor and H. Chudzynska, *J. Crystal Growth*, 1986, **77**, 13.
81. D. C. Bradley, H. Chudzynska, M. M. Faktor, D. M. Frigo, M. B. Hursthouse, B. Hussein and L. M. Smith, *Polyhedron*, 1988, **7**, 1289.
82. A. C. Jones, *Chem. Soc. Rev.*, 1997, **26**, 101.
83. A. C. Jones, *J Crystal Growth*, 1993, **129**, 728.
84. M. de Keijser and G. J. M. Dormans, *Mater. Res. Soc. Bulletin*, 1996, **21**, 37.
85. I. M. Watson, *Chem. Vap. Deposition*, 1997, **3**, 9.
86. J. Bloem, *J. Crystal Growth*, 1980, **50**, 581.
87. G. H. Gilmer and J. Q. Broughton, *Ann. Rev. Mater. Sci.*, 1986, **16**, 487.
88. J. A. Venables, G. D. T. Spiller and M. Hanbrucka, *Rep. Progr. Phys.*, 1984, **47**, 399.
89. A. Madhukar and S. A. Chaisas, in *CRC Crit. Rev. Soild State Mater. Sci.*, 1988, **14**, 1.
90. H. E. Hintermann, *Ann. C I R P*, 1982, **31**, 405.

91. S. Wolf and R. N. Tauber, in *Silicon Processing for the VLSI era* (Lattice Press, Sunnat Beach, CA, 1986).
92. G. Wahl, in *Chemical Vapor Deposition*, eds. M. L. Hitchman and K. F. Jensen, Academic Press, New York, 1989, Chapter 10, and refs. therein.
93. L. J. van der Pauw, *Phys. Tech. Rev.*, 1958, **20**, 220.
94. E. R. Nicollian and J. Brews, in *MOS Physics and Technology* (Wiley, 1982).
95. G. D. Wilk, R. M. Wallace and J. M. Anthony, *J. Appl. Phys.*, 2001, **89**, 5243.
96. S. Taylor, P. A. Williams, J. L. Roberts, A. C. Jones and P. R. Chalker, *Electron. Lett.*, 2002, **38**, 1285.
97. K. Kukli, M. Ritala, M. Leskelä, T. Sajavaara, J. Keinonen, A. C. Jones and J. L. Roberts, *Chem. Mater.*, 2003, **15**, 1722.
98. R. O'Kane, J. Gaskell, A. C. Jones, P. R. Chalker, K. Black, M. Werner, P. Taechakumput, S. Taylor, P. N. Heys and R. Odedra, *Chem. Vap. Deposition*, 2007, **13**, 609.